Technical Report
RAL-TR-97-075

Fast Neutron Irradiation of some APDs Proposed for Application in the CMS ECAL

J E Bateman K W Bell S R Burge A L Lintern A S Marsh E J Spill R Stephenson and M J Torbet

December 1997

COUNCIL FOR THE CENTRAL LABORATORY OF THE RESEARCH COUNCILS

Enquiries about copyright, reproduction and requests for additional copies of this report should be addressed to:

The Central Laboratory of the Research Councils
Library and Information Services
Rutherford Appleton Laboratory
Chilton
Didcot
Oxfordshire
OX11 0QX
Tel: 01235 445384 Fax: 01235 446403
E-mail library@rl.ac.uk

ISSN 1358-6254

RAL-TR-97-075

FAST NEUTRON IRRADIATION OF SOME APDs PROPOSED FOR APPLICATION IN THE CMS ECAL

J E Bateman, K W Bell, S R Burge, A L Lintern, A S Marsh, E J Spill, R Stephenson and M J Torbet

Rutherford Appleton Laboratory, Chilton, Didcot, OX11 0QX, U K.

9 December 1997

ABSTRACT

The results of a programme of measurements of the effects of fast neutron irradiation on the performance of various APDs proposed for the barrel ECAL in CMS are reported.

1. INTRODUCTION

A considerable program of work is in hand in a number of centres aimed at proving the viability of the APD as a scintillation light detector for the electromagnetic calorimeter (ECAL) on the CMS experiment at LHC. Some of this work has been summarised in reference [1]. One important requirement (among many others) is that the devices exhibit a useful electronic dynamic range of 10^5, which in turn demands a low electronic noise threshold. Measurements have shown [2] that with the best devices RMS noise figures (referred to the input) of 50 electrons or less can be achieved at room temperature. APDs are, however, very sensitive to dark current-induced shot noise since the avalanche process amplifies any dark current present in the silicon of the conversion region just as if it were signal. The fast neutron flux generated by the ECAL is expected to be of the order of $2x10^{12}/cm^2$/annum. Such levels of flux are known to cause increased dark current in silicon due to the creation of shallow traps which ionise readily at room temperature. Measurents made using a reactor facility at several centres have indicated a serious degradation of the noise performance of both types of APD in fluences comparable to one years running at LHC [1]. This report summarises the results (to date) of measurements on devices which have been irradiated with fast neutrons using the ISIS facility at RAL. The tally of devices tested included one EG&G APD (C30626E), but mainly has consisted of Hamamatsu APDs derived from their basic S5345 device in a development programme organised and funded by Dieter Renker at PSI.

2. THE ISIS FACILITY

At the start of the acceleration cycle of the sychrotron approximately 10% of the injector beam is not trapped by the RF. During the initial phase of the magnet ramp in ISIS this 10% lost beam of 72 MeV protons spirals in and impinges on a cooled graphite block, generating an intense flux of neutrons with an energy spectrum peaking at about 1MeV, falling by a factor of 5 at 0.1MeV and 10MeV. An endless chain is installed in the machine hall which can transport a sample can (80mm long by 50mm diameter) from the outside of the hall (via a ventilation shaft) to a position approximately 30cm above the collector. When ISIS is running at it's usual beam current (180 - 200μA) samples receive a flux of 10^{12} n/cm^2 in approximately 25 minutes. Accurate calibration of the fluence experienced by the sample is obtained by counting a cobalt foil included with the sample. The neutron spectrum and the calibration procedures are described in detail in reference [3]. It is estimated that the gamma dose in the test facility is approximately 10% of the neutron dose.

3. THE APD TEST FACILITIES

In order to operate the APD at a gain of 50 in the ISIS test facility a stand-alone HT unit which could operate viably in the neutron flux was designed. In order to use the ISIS "chain" facility the sample for irradiation must be contained in a cylinder 50mm diameter by 80mm long. Thus a miniature battery-powered HT supply was produced which could deliver the bias potential required (≈150V for the S5345 and ≈300V for the C30626E) with a droop of about 5V after a fluence of $3x10^{12}$ n/cm^2. This deficit was entirely due to radiation damage affecting the reference junction in the regulator chip used. While this bias deficit had little effect on the gain of the EG&G device, the Hamamatsu APDs (with their

5-10%/V gain vs bias coefficient) gain would drop significantly from the preset value of 50. A large bias resistor (1MΩ) was used to protect the APD from potential breakdown and variations in the dark current during the exposure further reduced the APD gain towards the end of the exposure period. In order to minimise these effects the fluence was fractionated with a maximum step of around $3x10^{12}n/cm^2$.

The APD measurement facility provides environmental and bias controls for the APDs under test. The environment is arranged to provide temperature control to better than 0.1C and adequate electrical isolation to prevent RFI adding to the intrinsic readout noise of a few thousand electrons (variable with the APD load capacitance). The operational temperature range is 0C to 30C.

An HT supply is provided capable of delivering a bias (measured across the APD) stable and controllable to a precision of 0.01V independent of load current or temperature. Current limitation is provided to protect against runaway and consequent damage.

Access is provided so that stimulating illumination from an LED (or an x-ray source) can be introduced. In the present tests a SiC LED (central wavelength 480nm) is used in DC mode with a current of 2.85mA. A perspex light guide is used to distance the LED from the APD to minimise capacitative cross-talk when the LED is driven by a short (15ns) pulse to simulate scintillation events. This means that the LED is not temperature controlled and its output shows a dependence on ambient temperature.

Two stations are provided for APDs (or for an APD and a calibration PIN diode), though in practice only one is used. Installing an APD takes approximately 10 minutes and a further 10 to 15 minutes are required to permit the temperature to stabilise before measurements can commence. The APD holder is designed to reproducibly align the active area of the APD with the beam of light from the LED. In practice the LED-induced photocurrent varies with an rms of about 4% due to this effect.

Electronic readout is provided by means of one of our standard charge preamplifiers followed by a shaping amplifier with CR-RC time constants of 35ns. This set-up delivers an rms noise performance of 900 electrons plus 27 electrons/pF of load capacitance. At full bias this shows a noise of 4680 electrons rms with the BC type Hamamatsu APD.

System noise is measured using an HP 3400A true rms voltmeter and the charge calibration is performed using a step pulse applied to a test capacitor (1pF) which has been cross-calibrated with an independently calibrated charge terminator of the type supplied with an Ortec 480 pulser.

4. THE TEST PROCEDURES

After the temperature probe on the APD mounting is observed to have stabilised five measurements are taken at a sequence of APD bias potentials. These are:

1. The APD current with the LED off (dark current) - I_D (nA)
2. The APD current with the LED on (photocurrent + dark current) - I_{DL} (nA)
3. The RMS noise voltage at the amplifier O/P with the LED off - V_{off} (mV)
4. The RMS noise voltage at the amplifier O/P with the LED on - V_{on} (mV)
5. The pulse height observed on a CRT at the amplifier O/P when 10^6 electrons are injected by means of test pulse into the preamplifier I/P - k ($mV/10^6e^-$)

The measurements are used to determine the desired device parameters as follows:

The GAIN: $$M(V) = \{I_{DL}(V) - I_D(V)\}/\{I_{DL}(30.00) - I_D(30.00)\} \quad \{1\}$$

where we assume that at V=30.00V the APD has unity gain. The unity gain photocurrent - $i_L = I_D(30) - I_{DL}(30)$ - is chosen to be approximately 20nA as a compromise between achieving an adequate precision at low gains and avoiding device self-heating at high gains.

The EXCESS NOISE FACTOR:

$$F(V) = 2.89\text{x}10^9 \{V^2_{on} - V^2_{off}\} / \{i_L M^2 k^2\} \quad \{2\}$$

Figure 1 shows a typical plot of the three parameters in which we are principally interested, the gain, the dark current and the excess noise factor. The capacitance of the APD (as a function of bias voltage) can be deduced from the measurements of "k" if this is required.

5. PRECISION IRRADIATION MEASUREMENTS

We applied the facility to the assessment of the response of a group of four Hamamatsu APDs made available to us by Dieter Renker. These are putative production devices (of a design selected via the previous round of tests) for the ECAL and are identified by the numbers BC20-23. We retained BC20 as a reference, unirradiated specimen and subjected the other three to a fluence of $2\text{x}10^{11}n/cm^2$ in the ISIS test beam. Initially, the essential parameters of all four devices were followed for 30 days; however, in the light of the results the follow-up programme was varied for the different devices.

The four devices have well-controlled operating parameters giving a gain of 43±1 at a bias of 180.00V with a capacitance of 140pF. Dark currents at this bias ranged between 2nA and 7nA.

As will appear below, the device instability which we encountered in our previous tests on the Hamamatsu APDs again plagued our measurement programme. This instability (characterised by a runaway dark current) seems to bear no relation to any radiation effects since BC20 (unirradiated) developed it and BC22 (irradiated) did not. The effect of the irradiation on the dark current did, however, point to a possible source of the breakdown. The completeness of the data set was affected by the failure of the wire bond to the anode terminal of BC23 about 390 hours after the irradiation.

5.1 The Neutron Irradiation

The fast neutron irradiation was carried out on the ISIS test facility. An exposure of five minutes provides a fluence of $2x10^{11}n/cm^2$. Calibration of the fluence is obtained from a cobalt foil activation procedure. A special version of the miniature battery powered HT supply was developed which permitted biassing of up to four APDs during the irradiation. For this test the three APDs (BC21,BC22,BC23) were biassed to 180V during the single 5 minute exposure. After irradiation the APDs were removed quickly to the measurement facility and measurement commenced within 1 hour. Subsequently, all measurements were executed at a temperature of 18.0C but storage was at ambient temperature (variable between 21C and 24C).

5.2 Results

5.2.1 Dark Current

Figure 2 shows the behaviour of dark current of the APDs at V=180.00V as a function of time after the neutron exposure. Typically the dark current rises from a few nA before irradiation to >200nA decaying initially with a short time constant (≈7 hours) and a longer one (8 -10 days). The initial measurement period is too short to reveal any significantly longer time constants at this stage so the long term component is simply fitted with a constant. Taking the fits for BC22 as an example we find that 17% of the active states generated by the irradiation belong to the short-lived (7hour) species, 37% to the intermediate species (9days) and 46% to the long-lived species.

Figure 3 shows the same curves for the dark current measured at V=30.00V. Here we see similar fractions in the various species but a significant difference is seen in the fit to the short time constant, typically 4h compared with 7h at V=180.00V.

The gap in the data set for BC21 (52h - 174h) is due to the onset of the dark current runaway process which we had already encountered in many of the Hamamatsu diodes (see below). After a conditioning schedule was devised the data set was continued. The bond wire connection in BC23 finally failed at 364h and the data set stops. Only for BC22 does a complete data set exist.

The centres generating the excess dark current can be characterised by plotting the logarithm of the dark current (at 30V) against 1/(273.15+T). Figure 4 shows the result with a value for the activation energy of the centres of 0.51eV. This value is half the band gap of silicon, the expected activation energy for thermal ionisation of bulk silicon.

5.2.2 Noise

Plotting the rms noise values recorded during the tests at a bias of 180.00V against the corresponding dark current (or dark + photocurrent) permits calibration of the noise response of BC22 to increasing dark current. Figure 5 shows that a fit of the form expected from theory is obtained (i.e. the noise $\propto\sqrt{\{\text{APD current}\}}$) and that the noise is dominated by the series noise generated by the 140pF capacitance of the APD.

5.2.3 Gain

Figure 6 shows the gain of BC23 as measured during the test period. The gain was much less stable than expected with a brief increase of about 2% just a few hours after the irradiation followed by an undershoot and recovery. Measurements had an rms noise of approaching 1% which is considerably in excess of our measurement errors and showed a correlation with the "runaway" episodes in the APDs affected. Within the noise, all three devices showed the same effect.

5.2.4 Excess Noise Factor

In order to compare with the basic statistical model it is usual to plot the excess noise factor as a function of the gain. Figure 7 shows such a plot for BC22 with data taken before and after the irradiation. It will be observed that data points are not plotted for M<10. This is due to the extreme noise sensitivity of equation {2} as M approaches unity from above. The fits make use of McIntyre's statistical model [4]:

$$F(M) = aM + (2 - 1/M)(1-a) \qquad \{3\}$$

where a is the ratio of the hole townsend coefficient to the electron townsend coefficient (normally $\approx$1%) and the number 2 represents an idealised electron multiplication process. Fits to this formula can be obtained if the figure 2 is replaced by a free fitting parameter "b" which is generally found to be in the region of 1.8. This parameterisation allows us to quantify any changes in F in a convenient mannner as is shown in figure 8. There seems to be no significant change in F after irradiation.

5.3 Results of a second irradiation

This section describes the continuation of the tests described above on APDs numbers 20-23 using the same facilities. The same pulse dose of fast neutrons of $2x10^{11}n/cm^2$ delivered in a period of approximately five minutes was given to BC21, while BC20 and BC22 were monitored for comparision.

Of the four APDs available at the start of the tests, BC20 had been reserved as an unirradiated reference device while the other three had a single pulse dose on 26 March 1997. The dark current, gain and noise were monitored for the following two months before the second dose pulse was delivered. During this period a bond wire failure occurred in BC23 leaving BC21 and BC22 in the programme. In order to detect any long (>6 month) time constant in the decay of the leakage current BC22 was not irradiated with a second pulse which was thus given only to BC21 on 3 June 1997.

Having only one temperature-controlled test station the APDs had to be rotated through the measuring facility. It was clear from the results presented in [1] that the biassing and unbiassing of the devices which thus resulted caused serious instability in the behaviour of the APDs and introduced uncertainties into the dark current and gain measurements. The chief aim of this phase of measurement was therefore to keep the conditions on the APD as stable as possible during the course of the measurements with a bias of 180.01±0.01V and a temperature of 18.0±0.1C. (Of course, the bias had

to be cycled briefly to perform the gain measurement as described in [1]). Thus, measurements were made in sequences of between one and three weeks duration in which the APD was constantly under bias and under thermostatic control. The runaway dark current problem was encountered with all three devices whenever newly biased, but all devices were stable by the next working day.

In the case of the second irradiation of BC21, the device was measured for two weeks under constant bias beforehand and was extracted from the test facility for only one hour for the irradiation, before being returned to the standard bias and temperature conditions. (During the irradiation it was under the standard bias but at ambient temperature of around 23C.) The subsequent measurements were then made under constant conditions for the following three weeks.

5.3.1 Dark Current Measurements

With the inevitable gap when the rig was occupied by BC21, the dark current of BC22 (at a bias of 180.01V) has been tracked up to 165 days after its single pulse dose on 26 March. Figure 9 shows the data obtained. Up to 500 hours the data was taken with the APD installed in the rig for just long enough for it to settle down before the measurent was taken. The groups taken after 750 hours were taken in continuous sequence with the device under constant conditions (after at least 48 hours under bias to settle down). In between the measurement sequences the device was stored at ambient temperature (≈21C) with no bias.

The multi-exponential fit shown in figure 9 shows that there is 17.8% of the induced dark current in a time constant of 8.39h, 34.9% in one of 259h, 14.6% in one of 2987h and 32.7% in a time constant long compared with our sample period. The fraction in this very long time constant (VL) is consistent with that observed in the devices H048 and H049 which were irradiated in January 1996 (see section 7 below).

In figure 10 the decay of the dark current of BC21 in the period before the second irradiation is seen to be similar to that of BC22 with 14% in the 2.4h time constant, 17% in the 37.9h, 31% in the 460.4h and 38% in the DC component.

After the second irradiation the corresponding figures are: 9.7% in the 4.7h component, 10.9% in the 54h component, 27.4% in the 812h component and 52% in the VL component. As expected the VL component has approximately doubled, showing the likely build up of dark current in a long irradiation at the rate of approximately $44nA/10^{11}n/cm^2$.

While the fraction of the signal in each component is much the same as before, there is a significant difference in the time constants which are between 1/2 and 1/5 of the values from the first irradiation. This possibly reflects the effect of the constant device temperature of 18.0C during the post irradiation period in the second instance, though, of course we have not attempted to correct for the underlying decay of the contribution from the previous irradiation which will tend to give shorter apparent time constants.

5.3.2 Gain Measurements

The five weeks of gain measurements on BC21 (two weeks before and three weeks after the second irradiation) are shown in figure 11 (note the negative slope of -0.0018/h). Superimposed on the linear decline are the noise from the temperature control and the characteristic short-term gain excursion previously observed after the pulse irradiation.

Normalising the data points in figure 11 to the linear fit yields a plot of the short-term excursion which can be compared with the excursion observed during the first irradiation (figure 12). While not identical, the two waveforms are clearly related and the positive excursion a few hours after irradiation in the second case does correspond with the much larger positive spike observed in the first irradiation. The errors in the second case are simply due to the 0.1C temperature uncertainty.

5.4 Gain Stability

The instability observed in the gain measurements (figure 11) calls into question the ECAL requirement for a gain stability of 0.25% (rms) in the channels. Figure 13 shows a similar pattern of erratic gain behaviour (outside the required limits) in the measurements on BC22. In the context of stable device conditions we anticipated gain values stable to within the limits set by our temperature control of ±0.1C, i.e. ±0.2%. Figure 13 shows the gain of BC22 measured in two sessions separated by five weeks. Contrary to expectations a systematic gain change is observed amounting to -0.0013/h superimposed on the 0.2% fluctuations caused by the temperature control. During the five weeks rest the gain seems to have recovered slightly and recommenced the steady decline under bias.

In order to separate out various possible effects not attributable to irradiation we arranged for BC20 (unirradiated) to be installed in the test facility and kept at 18.0C under fixed bias (180.00V) for two separate periods of one week and three weeks (before and after the measurements on the irradiated devices). This provides more realistic operating conditions and removes the possibility of effects due to the small variations in APD position giving differences in the average gain across the device aperture. Figure 14 shows the plot of the gain thus measured over this period.

The temperature coefficient of the gain of these devices was measured to be -2% /C at V=180, T=18C. With a resolution of 0.1C on our temperature control an error in the region of 0.2% would result. The gain/voltage coefficient was found to be +6%/V under the test conditions so that the resolution of 0.01V on the bias would result in a contribution of 0.06%. The observed rms error in the gain of BC20 in figure 14 is about 0.15% and is thus better than one would expect, probably due to the stable ambient temperature during the measurement period. Thus under conditions of constant bias the stability of the unirradiated APD BC20 (at least on this time scale) is within the specification required for application to the ECAL while the >1% excursions seen in the irradiated diodes put a question mark over their stability.

6. HIGH DOSE MEASUREMENTS

A group of devices were irradiated in graduated steps over a period of one month in the neutron beam up to the maximum fluence foreseen for 10 years of CMS operation: $2x10^{13}n/cm^2$. H048 and H049 were examples of the standard Hamamatsu APD (5mm active diameter) S5345 packaged in a flat pack rather than the usual metal can. The operating bias of these devices is 144V for a nominal gain of 50 and the device capacitance is 300pF. H048 was kept continuously under bias during irradiation and H049 was unbiassed (for comparison). At the same time an example of the EG&G APD type C30626E was irradiated under the same schedule. This device (E135) had an operating bias of 284V for a nominal gain of 50 and a corresponding capacitance of 30pF.

After the higher dose irradiations the test assemblies were quite radioactive so a period of 24 hours in storage was imposed before measurement of the APD characteristics commenced. At the period of these experiments the test-measurement facility was not available so that the temperature was not controlled either during storage or measurement and the bias control was a manual setting. It is estimated that room temperature fluctuated in the range 21 ±1C during the measurements. As a result of the instrumental limitations the data acquired was restricted to dark current and noise measurements.

Figures 15 and 16 show the raw dark current and noise (30ns CR-RC time constants) measured at 24 hours after each incremental irradiation for the three devices. H048 has a complete data set while the dose on H049 was fractionated in coarser steps (with a minimum of $3.5x10^{12}n/cm^2$). The curves for E136 (the EG&G device) stop at $2x10^{12}n/cm^2$ because on the next dose increment the dark current ran away to values of 50μA on the application of bias. The fault condition gradually healed itself and was traced to an edge leakage effect. After a further irradiation of $3x10^{12}n/cm^2$ the guard ring connection failed completely (see reference [2] for details).

Figure 9 shows that a substantial proportion of the neutron-induced dark current can be expected to decay during the 20 day period occupied by the high dose irradiations. It is clear from figure 4 that the dark current is an effect attributable to damage in the bulk silicon of the devices and that therefore the decay curve of figure 9 can be used to correct for the decay of the centres generated at each irradiation throughout the course of the measurements. Figure 17 shows the dark current corrected to t=0 (for each dose increment) as a function of the neutron fluence for H048 at a gain of 50. The sub-linear behaviour is probably just a result of the poor bias control in the face of the very large (20μA) dark currents encountered at the higher fluences. The dark current has no negative feedback effect on the signal at a bias of 30V (M=1). Figure 18 shows the corresponding (corrected) curve for this data. Here the neutron-induced dark current does fit quite well with a linear response model.

7. LONG DARK CURRENT DECAY TIME CONSTANTS

Figure 9 shows that under conditions of storage and operation close to ambient temperature the dark current induced by neutron irradiation has a very long (VL) component with a lifetime >>200 days. It was possible to return at intervals to the devices irradiated to $2x10^{13}$ n/cm^2 in January 1996 (H048 and H049) to check the dark current for this component. Figure 19 shows the data acquired. Fitting the data for H049 to two exponentials (there are insufficient data points to explore the intermediate time constants seen in figure 9) shows a VL component with a time constant of 1123.7 days (i.e. 3 years).

8. IRRADIATION OF SEVEN DEVELOPMENT DIODES

In a development campaign organised by Dieter Renker, Hamamatsu produced a series of ADPs with varied parameters from which the optimal specification would be selected for production. Seven different devices were tested in the ISIS facility to see if the process variations had any significant effect on the response of the dark current to neutron irradiation. The devices fell into three groups: BA4, BA4N, BB4 and BC4 operated at around 200V bias (capacitances in the range 120 - 140pF), BD4 and BE4 operated at around 120V bias (capacitances in the range 430 - 480pF) and BF4N operated at around 320V bias (capacitance around 120pF) when the gain was 50. Before irradiation the devices were characterised with respect to gain and dark current at a stabilised temperature of 24.6C.

The diodes were irradiated with $2x10^{11}$ n/cm^2 while under the bias required to give a gain of 50 at an ambient temperature of approximately 24C. The dark current and gain were monitored at 1, 8 and 120 days after the irradiation, all measurements taking place at 24.6C. In between measurements the diodes were stored at ambient room temperature. Table 1 summarises the results. The main feature of the results is that the diodes all respond to irradiation in a similar manner: there is only approximately a 10% variation about the mean 24-hour dark current of 284.6nA. Similarly the fraction of the 24-hour dark current remaining at day 120 is 0.48±0.05 and the single exponential (plus a constant) fit made to the three data points gives a decay time of 8.3±1.3 days for the six devices which survived the irradiation.

The missing entries for post-irradiation measurements on BF4N indicate the first occurrence of the biassing instability problem encountered eventually with all the Hamamatsu diodes tested. On the application of bias after a period (> few hours) off bias) the dark current would run away at quite a low bias voltage so that it was impossible to reach a gain of 50. It was found (by Dieter Renker) that leaving the device drawing several microamps of current (with suitable current limitation in the circuit) led to an eventual recovery and normal operation. The period required varied from device to device ranging from the order of 30 minutes to several hours. Since both gain and dark current exhibited some instability in the hours following the application of bias the practice was adopted of leaving a device for 24 hours under bias before commencing measurements. Unfortunately it was found that after irradiation BF4N would not respond to the "conditioning" treatment; hence the gaps in Table 1.

At 120 days post irradiation the gain and dark current of BD4 were measured as a function of temperature. At 18C 1/MdM/dT was found to be 3.6% and a plot of the ln(dark current) versus 1/T at M=1 gave an activation energy of 0.532eV (i.e. half the band gap of silicon)

9. A LONG-TERM IRRADIATION FACILITY

The dose rate delivered to the APDs in the ISIS "chain" facility used for the tests so far described is approximately 5000 times that anticipated in the ECAL on CMS. While convenient for high dose measurements, the question remains as to whether there is any dose rate effect. To answer this problem a facility has been developed such that the the dark current of an APD can be monitored under controlled bias and temperature conditions while installed on the floor of the ISIS beam hall about 2 meters from the beam collector where the neutron flux is only about 3 times that expected in the ECAL. Operation must be totally remote since access to the station is limited to periods of ISIS shut-down. Calibration of the neutron fluence was carried out (as usual) by means of a cobalt foil placed beside the APD.

The facility was installed just before the first ISIS cycle of 1997 and APD #BC4, biassed to a nominal gain of 50 and held at 18.0C was exposed through three machine cycles. The data from cycles 1 and 3 are shown in figure 20 (the data from cycle 2 was lost through equipment failure). Fitting straight lines to the two periods gives a consistent dark current increase rate of 2.4×10^{-18} A/(n/cm^2). The line segments do not line up because of the two week shut downs between the cycles when the dark current decays.

Figure 21 shows the dark current data from cycle 1 fitted with the expected growth curve derived from the decay curve measured from BC22. The daily neutron flux was estimated by combining the total fluence measured by the cobalt foil over the whole cycle (1.22×10^{12} n/cm^2 for E>10keV) with the ISIS daily beam current integrals. Dividing this number by the length of cycle 1 (30 days) we estimate a dose rate of 1.68×10^{9} n/cm^2/h which is 3.6 times dose rate expected in the ECAL at full luminosity. The anomalously sharp rise in the dark current at the beginning of the cycle is probably due to large beam losses as the accelerator is recommissioned after shut down.

10. DISCUSSION

10.1 Dark Current Mechanisms

Comparing the dark current curve in figures 2 and 3 one observes that the neutron-induced dark current at a gain of 50 is 100 times the dark current induced at a gain of unity; in an ideal device it should be only 50 times higher. Possible explanations are field-enhancement of the dark current and edge currents. A plot of the dark current divided by the gain ($z=I_D/M$) as a function of V_B was proposed as a diagnostic for possible field enhancement of the dark current at high gains . This effect does not seem to be present since z tends to decrease at high gains rather than increase as this model

would require. However, this plot is sensitive to the edge current of the APD. Figure 22 shows plots of this parameter for APD BC22 before and after its fast neutron dose. One can interpret the (no-dose) curve as follows. At V_B=30V (M=1) the dark current is dominated by the bulk leakage current. As V_B increases the edge current rises faster than the gain increase so that I_D/M increases until the gain reaches the steep part of its curve. Then z starts to decline. If the edge current is small compared with the gain-amplified bulk current then z returns roughly to its starting value. As figure 22 shows, this is the case except for the obvious incipient run-away exhibited by the last point at V_B=190V.

After neutron irradiation the situation is quite different (figure22). Even at V_B=190V (M≈90) z remains 2.5 times its starting value. This hints strongly that about 60% of the dark current induced by the neutron flux is flowing at the edges of the APD.

The parameter u = $I_D(V_B)$-MI_D(30) should (on our model) represent the current flowing at the edge of the APD. Figure 23 shows u plotted for BC22 before and after irradiation. Before irradiation u remains under control (increasing very slowly) except at V_B=190V when the runaway problem appears. After irradiation, not only is the dark current dramatically increased but it shows a response very similar to the gain curve. This would seem to indicate that amplification is now taking place in the edge region of the APD.

10.2 The Neutron Sensitivity of the Dark Current

We now have four distinct sets of measurements on the dark current induced in the Hamamatsu APDs. Unfortunately the detailed conditions vary making exact comparison difficult; however, we have enough information to correct for temperature differences and draw some conclusions:

(i) BC21, BC22, BC22

The average dark current (t=0) generated in these devices was approximately 224nA for $2x10^{11}$n/cm^2 (figure 2) giving a constant of **$1.12x10^{-18}$A/(n/cm^2)** (at 18.0C).

(ii) H048, H049

The decay-corrected dark current curve for H048 (figure 19) yields a slope of 192nA/10^{11} n/cm^2. These measurements were performed at an ambient of about 21C and the current can be approximately corrected to 18C using the dark current versus temperature curve measured for BD4. This reduces the constant to **$1.55x10^{-18}$A/(n/cm^2)**.

(iii) BA4,BA4N,BB4,BC4,BD4,BE4

The six prototype devices measured at 24.6C and 24 hours after irradiation showed an average (±10%) of 284.6nA for $2x10^{11}$ n/cm^2 (table 1). Correcting this to 18C gives 178nA and a constant $0.89x10^{-18}$ A/(n/cm^2). If we make the reasonable assumption that the decay curve of BC22 is applicable and correct this number back to t=0 from t=24h then we find a constant of **$1.17x10^{-18}$ A/(n/cm^2).**

(iv) BC4 in Long Term Facility

Fitting the dark current generated in BC4 (T=18.0C, M=50) in the first ISIS cycle (figure 21) to the growth curve predicted by the detailed decay observed in BC22 (figure 2) (see below for details) yields a constant of **4.13×10^{-18} A/(n/cm^2).**

(v) E135 (EG&G)

The first pulsed dose of 2×10^{11} n/cm^2 on this device yielded a dark current of 370nA measured at t = 24h. This equates to a sensitivity constant of **1.85×10^{-18} A/(n/cm^2)** at t=24h (M=50, T=21C).

Thus, from the "chain" measurements we obtain a reasonably consistent sensitivity constant for the Hamamatsu diodes (M=50, t=0) of just over 10^{-18}A/(n/cm^2). The EG&G seems to be considerably worse - if one scaled the t=24h current back to t=0 using the BC22 model then the constant would be double the average for the Hamamatsu devices under pulsed irradiation. The explanation of the much larger constant when a Hamamtsu device is irradiated in the long term facility is not obvious; future measurements in the facility should help to clear up the problem.

10.3 The Dark Current Decay Profile.

The dark current decay profile is important to the extent that it helps to determines the build-up of the dark current in the steady irradiation conditions in the ECAL. As figure 2 shows the response of the dark current of the three production diodes tested was consistent within about 10%. It is thus plausible to take the dark current decay curve obtained for BC22 over 165 days to represent all BC devices. This measurement period is not long enough to characterise the VL time constant which is obviously present. The VL time constant derived from the long term data obtained from H049 is quite compatible with the BC22 data and can be incorporated in the fit to give an estimate of the complete decay out to times of the order of 18 months. The result of the fit (normalised to unity at t = 0) is:

$$F_D(t) = 0.172e^{-t/7.7} + 0.230e^{-t/191} + 0.174e^{-t/528} + 0.425e^{-t/26970} \qquad \{4\}$$

where time after irradiation (t) is in hours. This decay profile refers to the situation where the APDs are maintained at a temperature of around 20C during most of the time with measurements made at 18C.

10.4 Dark Current Build-up

If we allow the validity of treating the various fitted exponential distributions in the dark current decay curve as independent physical processes then it is possible to model the build-up of the dark current under conditions of constant irradiation. For each component we can write down the following differential equation:

$$dI_i/dt = f_i g D - I_i/\tau_i$$

where I_i is the value of dark current component (i), f_i is the fraction of the dark current in this component at t=0 and τ is the time constant of the component, g is the sensitivity constant of the device ($A/(n/cm^2)$ at t=0) and D is the neutron flux ($n/cm^2/hr$). Integrating this we have:

$$I_i = \tau_i f_i g D (1 - e^{-t/\tau_i}) \qquad \{5\}$$

Summing over all the components we get:

$$I_D = gD\{\Sigma f_i \tau_i (1 - e^{t/\tau_i})\}$$

or: $$I_D = gDF_g(t)$$

where: $$F_g(t) = \Sigma f_i \tau_i (1 - e^{t/\tau_i})$$

is the growth function which can be evaluated from the dark current profile derived from BC22 {4} above. The growth function is plotted in figure 24 where it is observed that soon after 1000 hours after switch-on the growth of the dark current becomes linear as the shorter time constants saturate. From {5} above we see that the saturation contribution to the dark current is measured by the product $f_i\tau_i$. Evaluating these gives values of 1.32, 43.93, 91.87 and 11462 for the four components of the dark current. In one six month LHC cycle the VL component will reach an "ft" value of 1833.1 which is 13.4 times the dark current generated by the all the shorter components. It is thus clear that in respect of the deterioration of the dark current over time the VL component is the dominant concern.

10.5 The Electronic Noise

In the case of the Hamamatsu BC devices the electronic noise is dominated initially by the effect of the 140pF capacitance of the APD. The effect of neutron-induced dark current does not become significant until a dose of $5x10^{11}$ n/cm^2 has been accumulated. Using the fit of the noise to dark current (figure 5) and modelling the effects of continuous irradiation combined with the growth function of figure 24 one can estimate the growth of the dark current and the noise for any given LHC schedule. In figure 25 we have assumed a neutron fluence of $2x10^{12}$ n/cm^2 uniformly delivered in an LHC calendar year consisting of three beam periods of 60 days separated by 10 day rest periods with the remainder of the calendar year filled up with heavy ion running (assumed not to contribute to the neutron dose) and shut down [1]. The neutron sensitivity constant is taken to be $1x10^{-18}$ $A/(n/cm^2)$ as evaluated for the Hamamatsu devices in pulsed irradiation. The curve of I_D in figure 25 reproduces the main feature discussed above - namely that the build-up of the dark current is controlled principally by the VL time constant (3 years). The dark current saturates (at the end of the 10 year lifetime of the experiment) at about 2500nA and the corresponding noise figure is around 10000 electrons.

Inserting the neutron sensitivity factor obtained in the long term irradiation facility gives the growth curves plotted in figure 26 where we observe a saturation dark current of 10000nA and a saturation noise figure of 18000 electrons.

Our limited experience with the EG&G device (E135 - figures 15,16) showed that in the face of the neutron-induced dark current (and noise) there was no long term benefit in the initially low noise figure obtainable (≈1000 electrons) with this device. After a fluence of $2x10^{12}$ n/cm^2 (corresponding to the first year of full luminosity operation of the ECAL) the noise level was essentially the same as that of the high capacitance Hamamatsu devices (≈10000 electrons).

10.6 Gain Stability

One of the strong findings of these tests is that the Hamamatsu APDs must be left continuously biased for stable operation. In this condition they seem to be able to meet the requirement of 0.25% stability provided the temperature is stabilised (or monitored for offline correction) to better than 0.1C - as BC20 shows in figure 14. Unfortunately, after irradiation BC22 showed a gain instability with excursions of the order of 1% which would not be acceptable (figure 13). The effect is seen in BC21 and BC22 after irradiation but it does not appear to be proportional to the dose received since, as figure 11 reveals, the steady decline of the gain continues after the transient caused by the second irradiation of BC21 with no obvious change.

Since the gain measurement made according to formula {1} is self-normalising against calibration errors in the test equipment, and since the unirradiated BC20 does not show the effect, it must be concluded that the gain instability observed in BC21 and BC22 is a real effect of the neutron irradiation and therefore a cause for concern.

As figure 12 shows, the gain of the APDs does show a transient effect of the irradiation process; however, transient excursion in the gain seems likely to be an effect of the high dose rate applied (about 5000 times the dose rate expected in practice) and may not be significant in the low flux experienced in the ECAL.

10.7 Excess Noise factor

The excess noise factor in the Hamamatsu prototypes shows no unexpected behaviour under neutron irradiation at the level of $2x10^{11}$ n/cm^2. The electronic noise parameter (b) averages to 1.78 and the hole/electron ratio (a) averages to 0.0095. These values are both rather lower than expected and this could reflect an electronic calibration problem, though we believe our charge calibration to be good to about 2% and a 10% error is required to account for the difference. One must also take account of the fact that the model of the avalanche process is rather approximate.

11. CONCLUSIONS

Of the 14 APDs irradiated in the ISIS facility at RAL, 11 devices survived varying doses of fast neutrons up to a total (in two cases) of $2x10^{13}$ n/cm^2. One had a mechanical package failure (BC23), one exhibited irretrievable runaway dark current after $2x10^{11}$ n/cm^2 (BF4N) and one showed similar symptoms after $2x10^{11}$ n/cm^2 (E135). When irradiated in pulsed mode on the "chain" facility the Hamamatsu diodes showed a fairly consistent dark current sensitivity constant of ≈$1x10^{-18}$ A/(n/cm^2) at

t=0. But when installed in the long term facility with a dose rate approximately three times that expected in the ECAL (instead of x5000 in the "chain" facility) one of the protoype devices exhibited a constant about four time greater. If this is a genuine effect of the lower dose rate, then this is a matter for concern.

The decay profile of the neutron-induced dark current was observed to be similar in all the diodes tested. Considerable variation is observed in the short time constants (up to one month) but in all cases we find roughly 40% of the dark current persisting with a time constant which is of the order of 3 years. It is this VL time constant that, in the end, determines the build-up of dark current (and hence noise) in the APDs during the lifetime of LHC. By the end of the second year of full luminosity operation the electronic noise of a BC type device will have climbed from around 4000 electrons to 8000 electrons (rms) (assuming that the low neutron sensitivity constant of the pulsed irradiations is valid).

On first encountering the run-away behaviour of the Hamamatsu APDs we conjectured that the effect was caused by the packaging. The results presented in figures 22,23 seem to indicate quite strongly that the large currents are generated in the silicon at the edge of the active area. In particular we find:

- It appears that 60% of the neutron-induced dark current flows at the edges of the APD.
- All the neutron-induced dark current fits a temperature curve which yields an activation energy of half the silicon band gap; i.e. the dark current is generated in silicon.
- The irradiation process radically changes the V/I characteristic of the edge current.
- The short dark current recovery time constants are quite significantly different in the case of unity gain (essentially bulk current) and M=43 (with a large contribution of edge current). Compare figures 2 and 3.

The gain stability of the BC class of devices appears to be adequate to meet the ECAL specification in the case of unirradiated devices. However, the random excursions (of order 1%) seen in the gain of BC21 and 22 after irradiation indicated considerable cause for concern. The transient gain shifts seen in the pulsed irradiations are probably not significant due to the artificially high dose rate.

It is possible that the gain instabilities and excessive dark current effects are due to a common cause in the edge structure of the APD where a localised high gain region may be amplifying both the light signal and dark current induced in the peripheral silicon.

ACKNOWLEDGEMENTS

We would particularly like to thank our colleagues Mike Edwards and Derrick Hill in Particle Physics Department and the ISIS operations staff for their help with the irradiations.

REFERENCES

[1] CMS - The Electromagnetic Calorimeter, Preliminary Design Report.

[2] Gain and noise measurements on two avalanche photodiodes proposed for the CMS ECAL, J E Bateman, S R Burge and R Stephenson RAL-TR-95-001.

[3] The Radiation Hardness Test Facility, M Edwards and D R Perry, RAL-90-065

[4] R J McIntyre, IEEE Trans Elec Dev ED-13 (No.1) 1966, 164

APD #	BiasVoltage (M=50)	1/MdM/dV (V^{-1})	Dark Current nA t = -1 day	Dark Current nA t = +1 day	Dark Current nA t= +120 day
BA4	192.7	0.0715	30.1	278.3	148.0
BA4N	191.1	0.0682	3.0	303.6	151.0
BB4	199.4	0.0660	16.6	332.6	142.6
BC4	184.0	0.0803	5.9	300.5	154
BD4	119.2	0.185	32.4	273.5	113
BE4	111.7	0.291	19.6	318.5	165
BF4N	325.8	0.0617	3.7	-	-

TABLE 1

FIGURE CAPTIONS

Fig.1 The gain, dark current and excess noise factor measured as a function of the bias potential for APD BC22 before irradiation.

Fig.2 The dark currents of the three irradiated APDs as a function of time after irradiation with $2x10^{11}$ n/cm^2(measured at a bias of 180.00V).

Fig.3 The dark currents of the three irradiated APDs as a function of time after irradiation with $2x10^{11}$ n/cm^2(measured at a bias of 30.00V).

Fig.4 The thermal activation curve for the neutron-induced dark current in APD BC22 - measured at M=1 to avoid the confusing effect of the temperature dependence of the gain.

Fig.5 The rms noise (electrons) is plotted against the dark current for APD BC22 at V=180.00V, T=18.0C over the course of the tests. The two groups of points correspond to the two cases: LED off and LED on.

Fig.6 The gain of APD BC23 as a function of time from before the irradiation (at t=0) to 380 hours post iradiation.

Fig. 7 Excess noise factor versus gain plots for APD BC22 before and after irradiation.

Fig.8 The a and b parameters of the fits to the modified McIntyre model for the excess noise factor plotted throughout the period of the tests (irradiation at t=0).

Fig.9 The dark current of APD BC22 monitored for 165 days post irradiation with $2x10^{11}$n/cm^2.

Fig.10 The dark current of APD BC21 monitored for 150 days with an irradiation of $2x10^{11}$n/cm^2 at t=0h and t=1655h.

Fig.11 The gain of APD BC21 when maintained under constant bias (180.00V) and temperature (18.0C) for 28 days with the second dose of $2x10^{11}$n/cm^2 at t=1655h.

Fig.12 The gain data of figure 11 with the linear decline normalised out so that the gain excursion on the second irradiation can be compared with the average of the data obtained from APDs BC21,22,23 in the first irradiation.

Fig.13 The gain of APD BC22 when maintained under constant bias (180.00V) and temperature (18.0C) after one dose of $2x10^{11}$ n/cm^2 at t=0. Between the two data sets the device was held unbiassed at ambient temperature.

Fig.14 The gain of APD BC20 (unirradiated) measured under constant conditions in two periods approximately two and a half months apart. The gap on the time axis has been elided for clarity.

Fig.15 The dark current of the three devices exposed to high neutron fluences (up to $2x10^{13}n/cm^2$) as measured approximately 24 hours after each fraction of the accumulated fast neutron fluence.

Fig.16 The electronic noise measured in the amplifier system (30ns CR-RC shaping time constants) with the three devices exposed to high neutron fluences (measured 24 hours after each fraction of the accumulated fluence).

Fig.17 The dark current induced in H048 as a function of the accumulated neutron fluence (corrected to t=0 of the decay curve). (M=50)

Fig.18 The dark current induced in H048 as a function of the accumulated neutron fluence (corrected to t=0 of the decay curve). (M=1)

Fig.19 The dark currents of the Hamamatsu APDs, H048 and H049 measured out to 18 months after their irradiation to $2x10^{13}$ n/cm^2.

Fig. 20 The dark current monitored in BC4 as a function of the cummulative neutron fluence experienced in the long term irradiation facility.

Fig. 21 The dark current monitored in BC4 in the long term irradiation facility as a function of time during the first ISIS cycle of the exposure.

Fig.22 The parameter $z = I_D/M$ plotted as a function of the bias potential for APD BC22, before and after irradiation.

Fig.23 The parameter $u = I_D(V) - MI_D(30)$ plotted as a function of the bias voltage.

Fig.24 The growth function for the dark current in a BC type APD under constant irradiation.

Fig.25 A model of the expected growth of the dark current and rms noise of a Hamamatsu BC type APD (M=50, T=18C) under the condition of a fluence of $2x10^{12}$ n/cm^2 being delivered in the proposed annual cycle of LHC running. The dark current neutron sensitivity constant (g) is that derived from the pulsed irradiations.

Fig.26 A model of the expected growth of the dark current and rms noise of a Hamamatsu BC type APD (M=50, T=18C) under the condition of a fluence of $2x10^{12}$ n/cm^2 being delivered in the proposed annual cycle of LHC running. The dark current neutron sensitivity constant (g) is that derived from the long term irradiations.

FIGURE 1

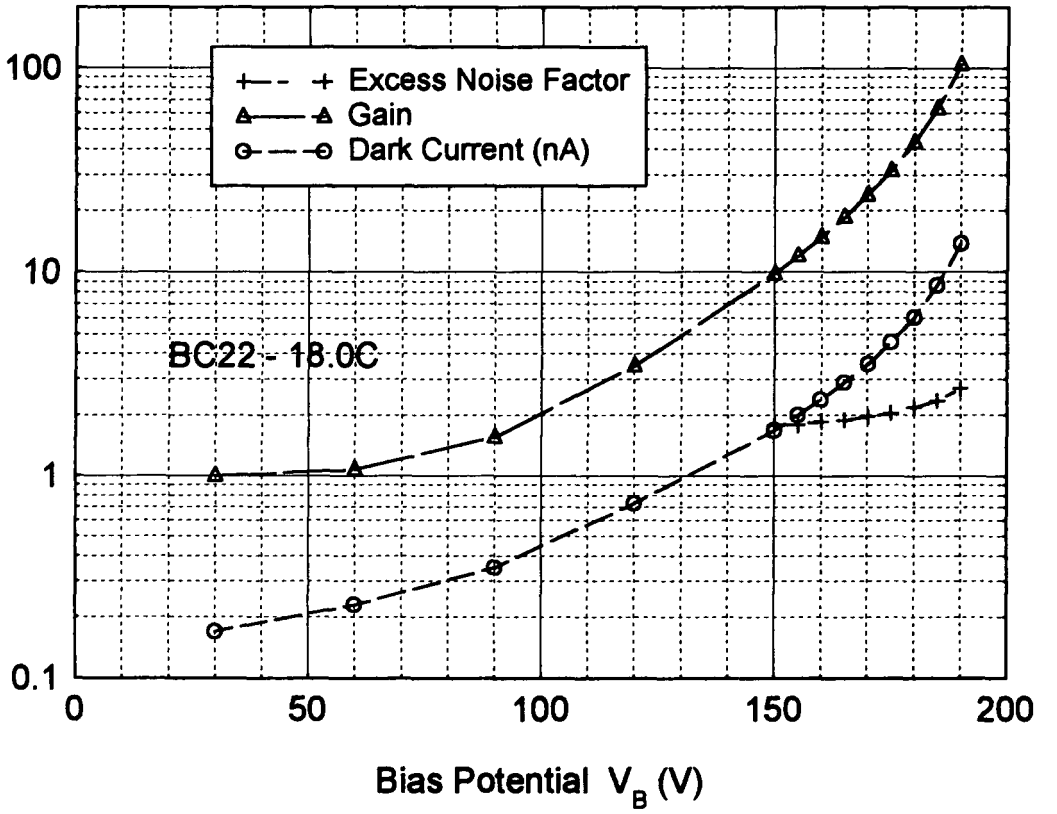

FIGURE 2

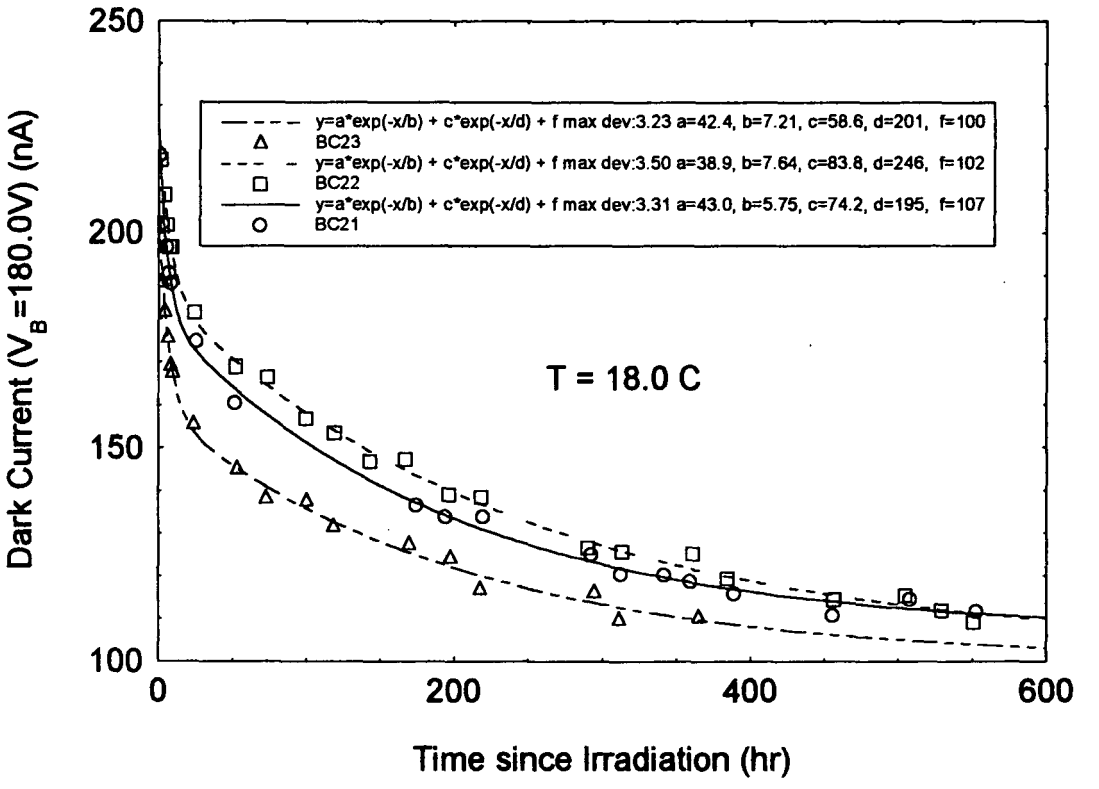

FIGURE 3

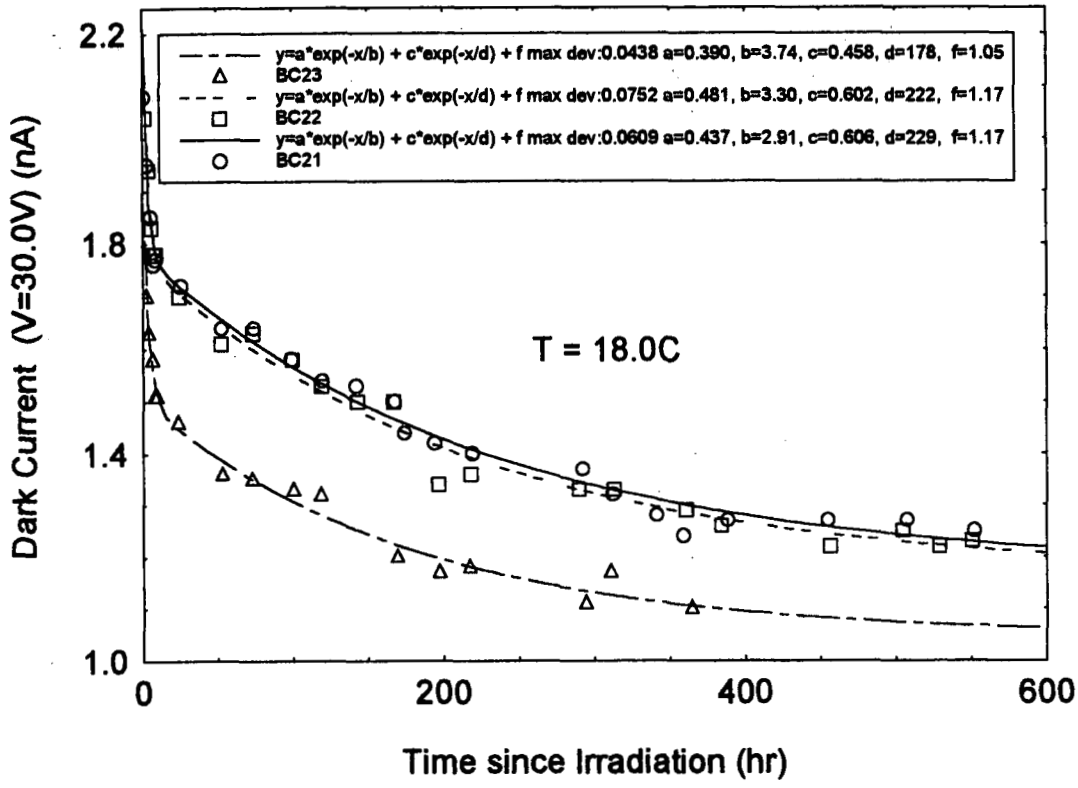

FIGURE 4

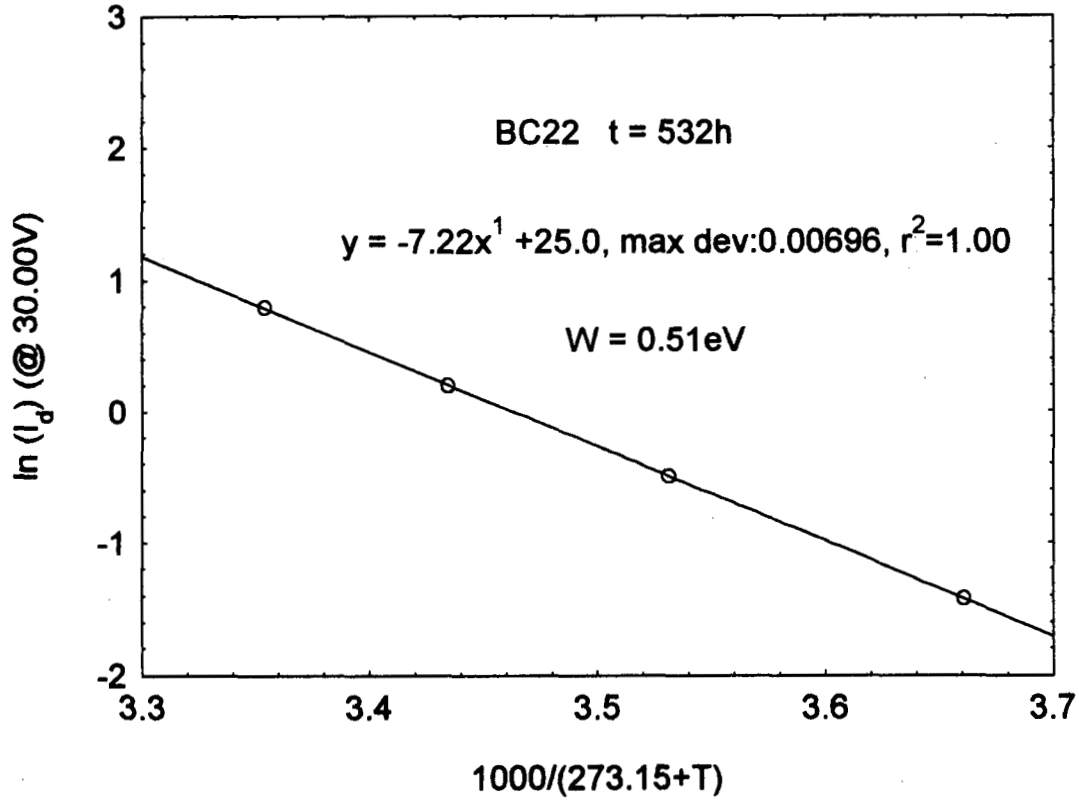

FIGURE 5

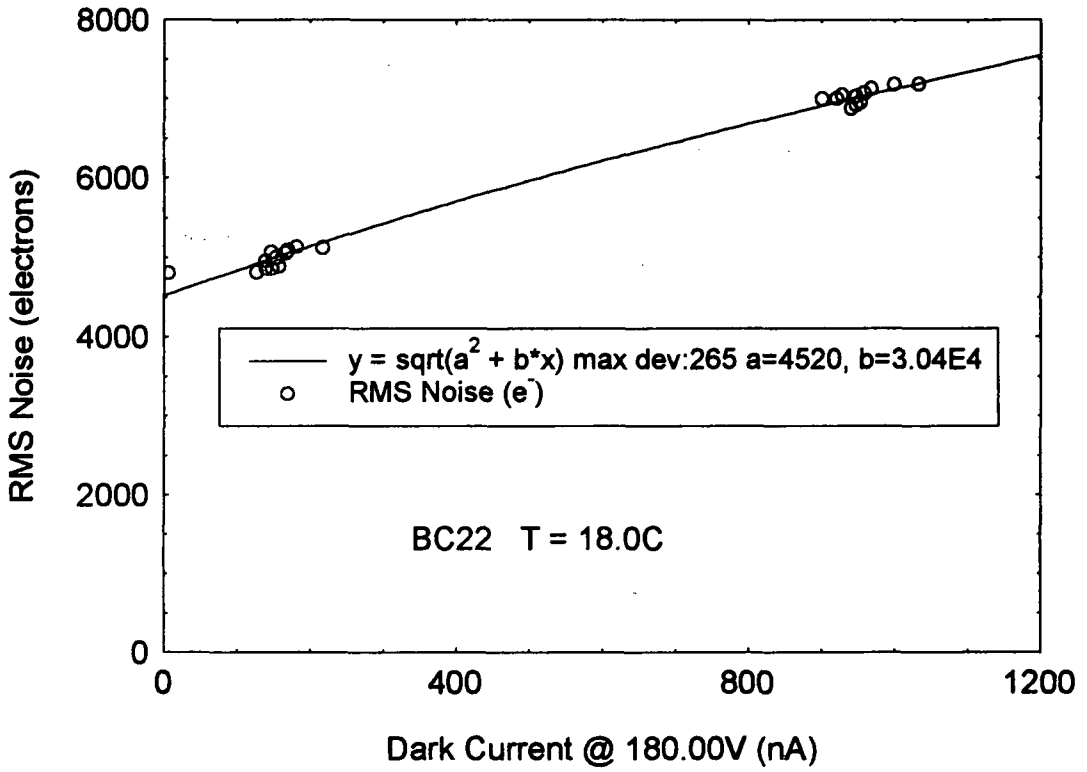

FIGURE 6

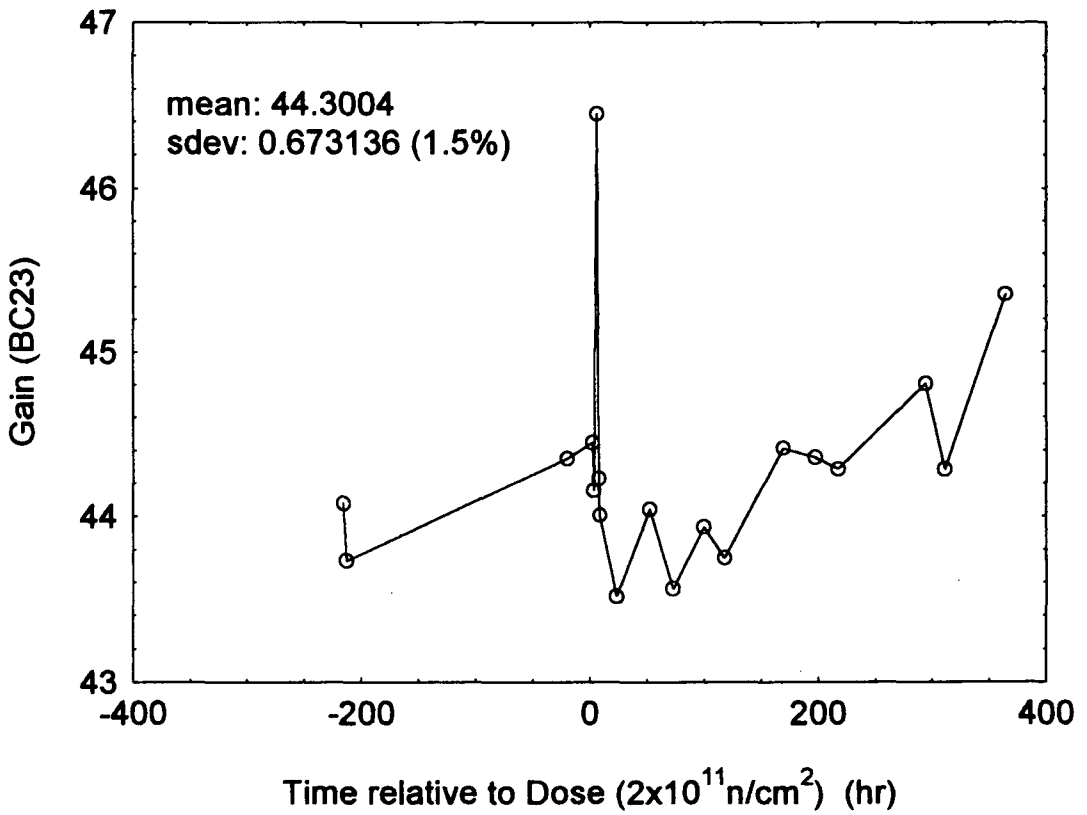

FIGURE 7

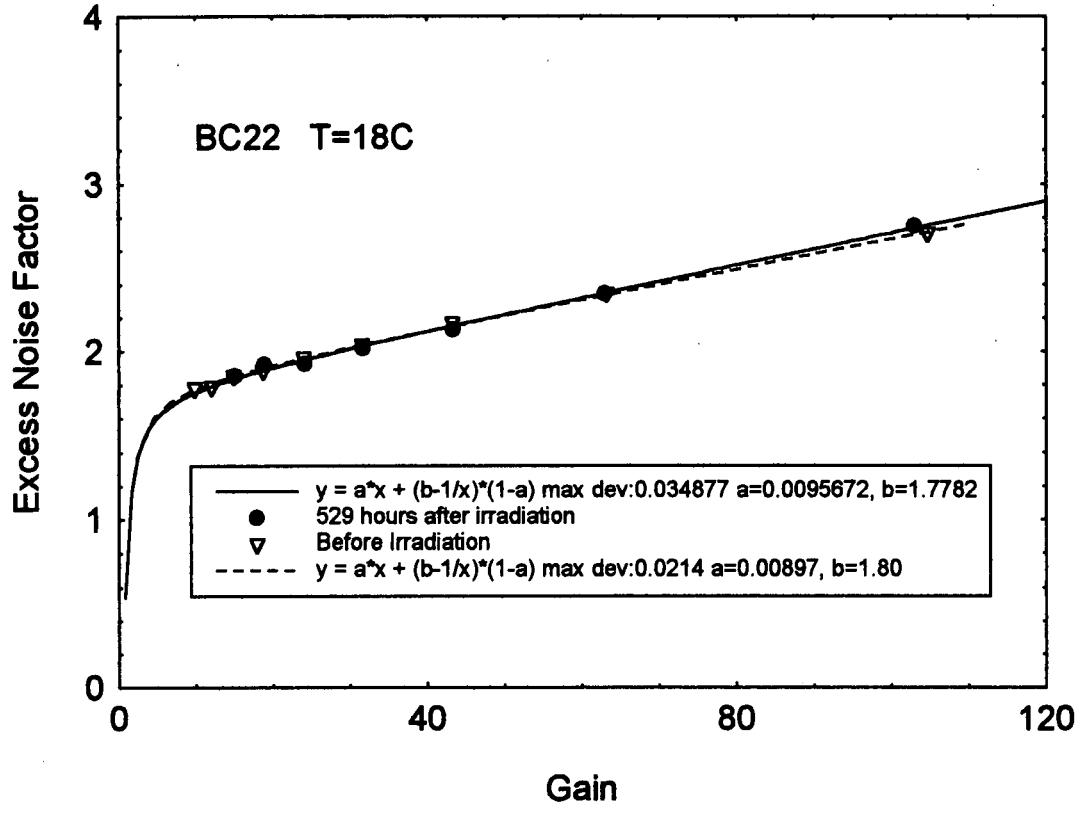

FIGURE 8

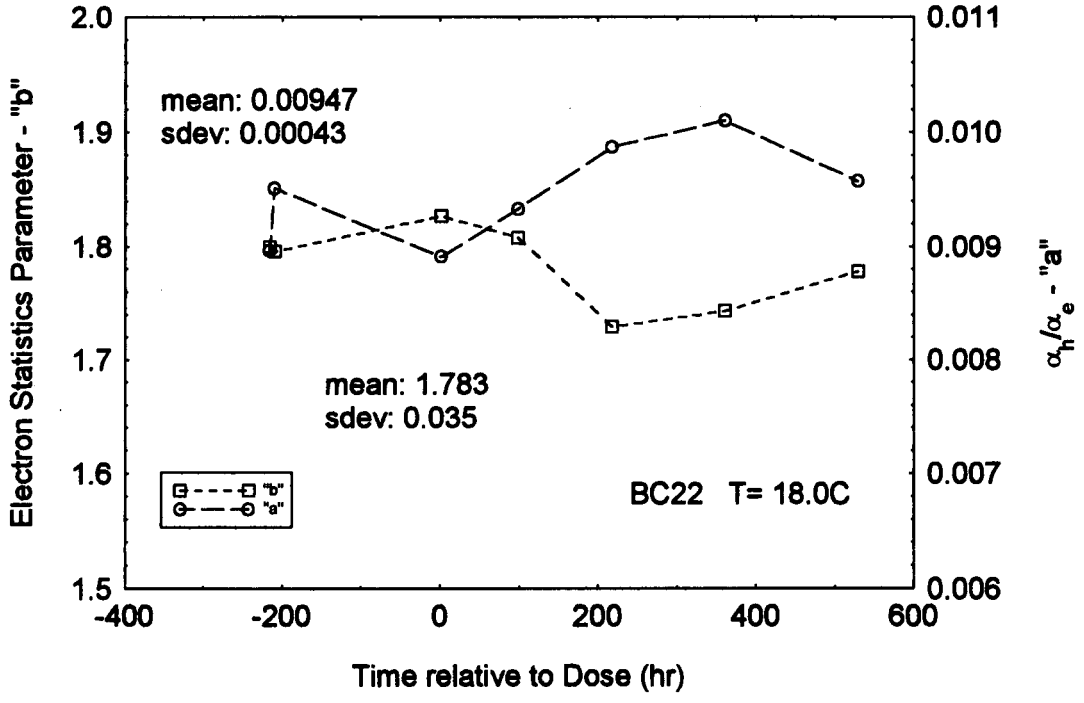

FIGURE 9

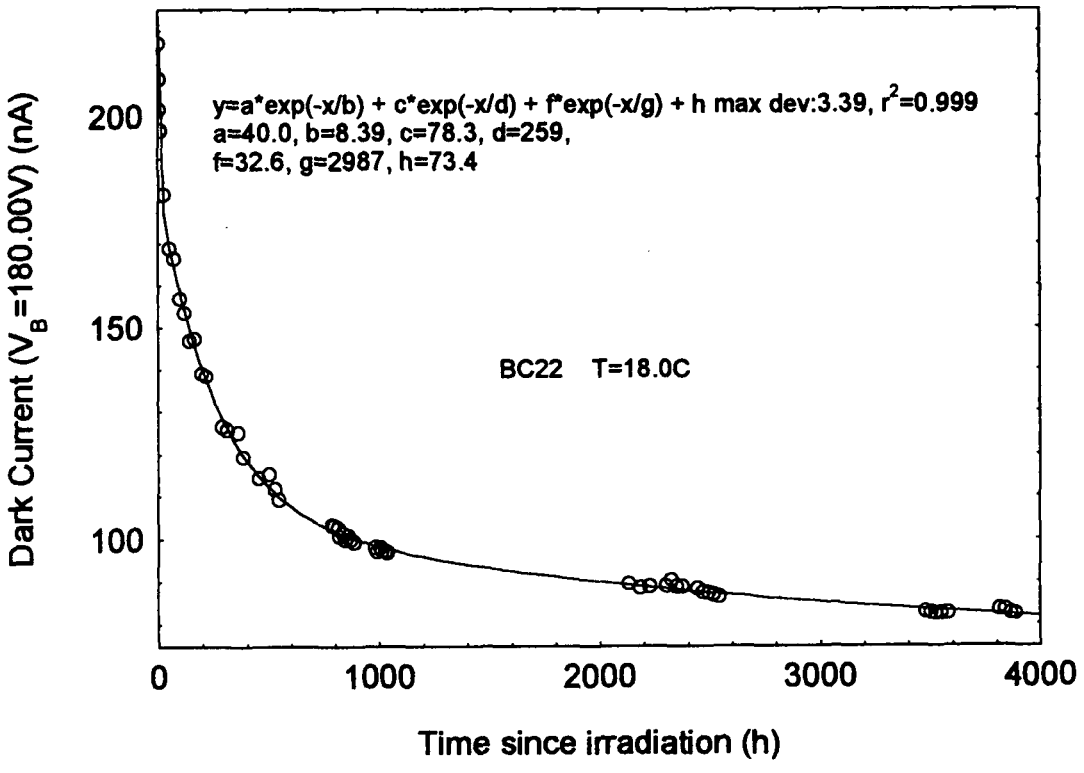

FIGURE 10

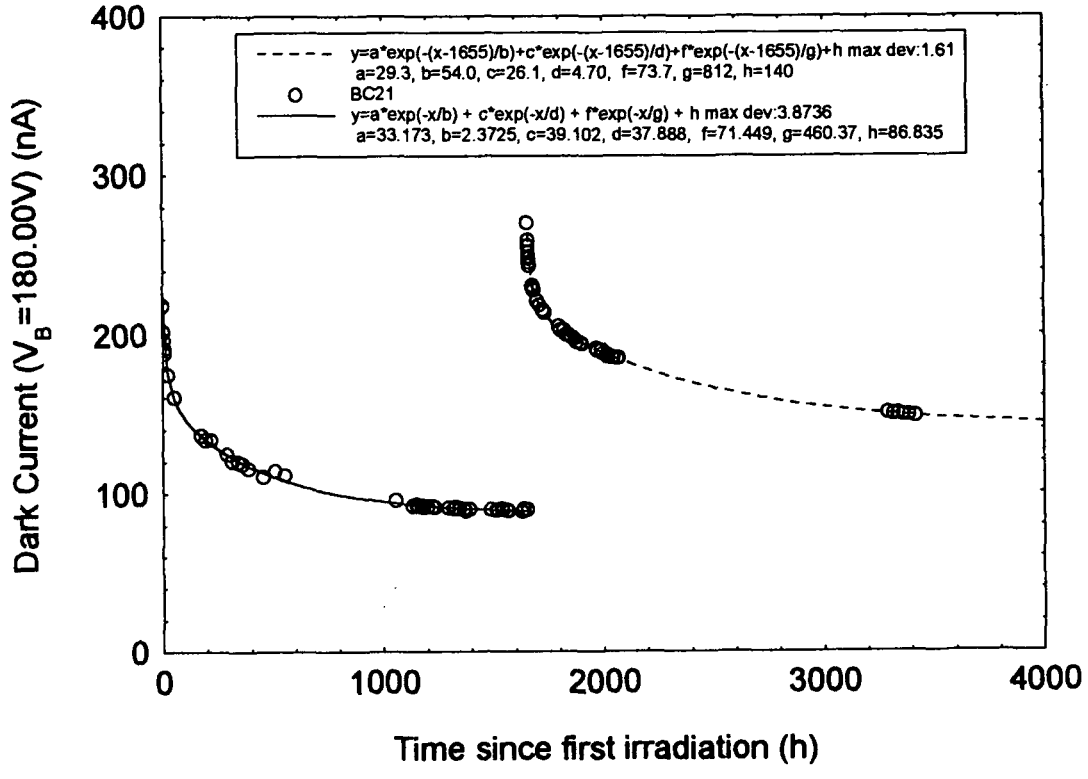

FIGURE 11

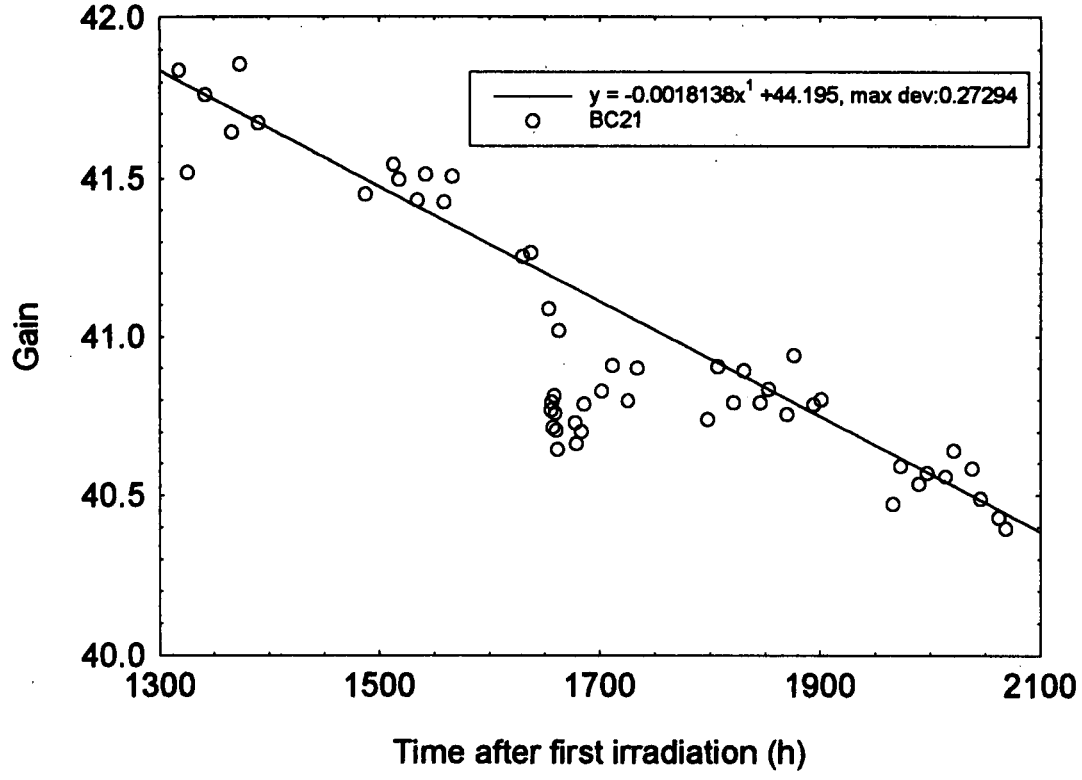

FIGURE 12

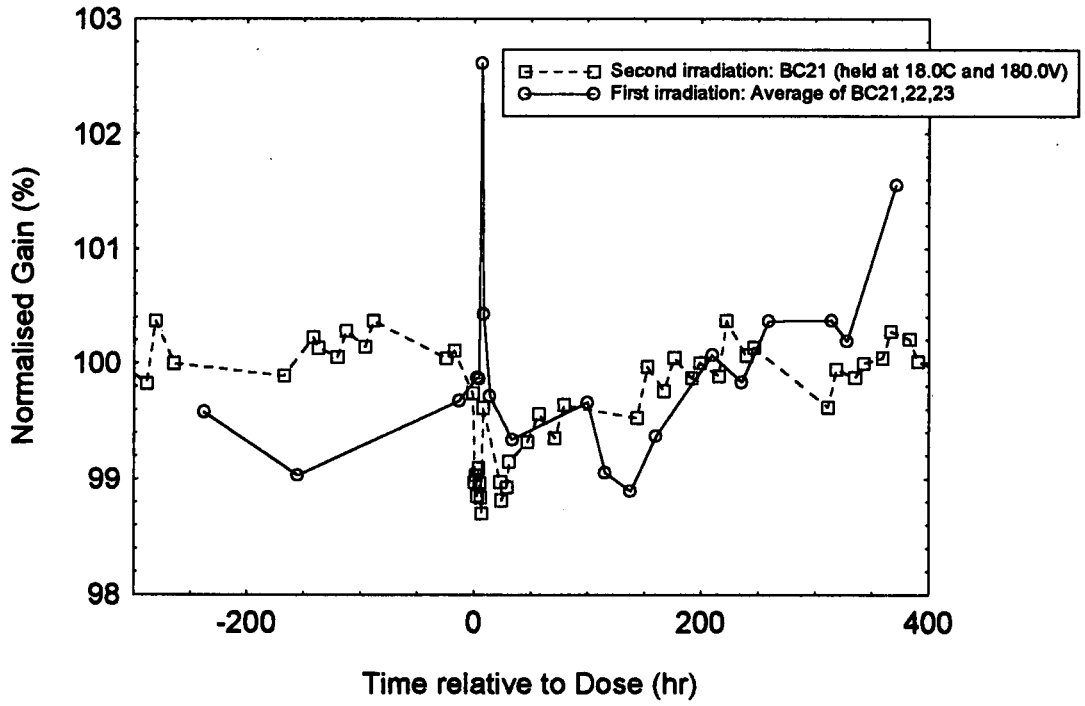

FIGURE 13

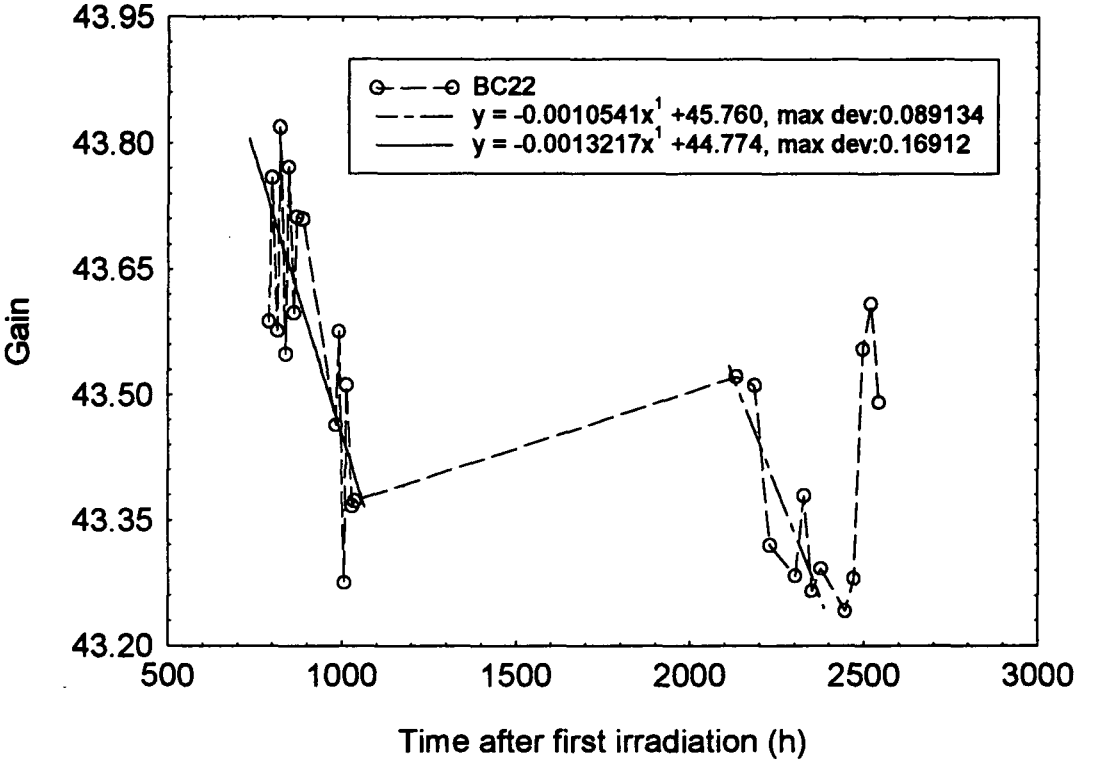

FIGURE 14

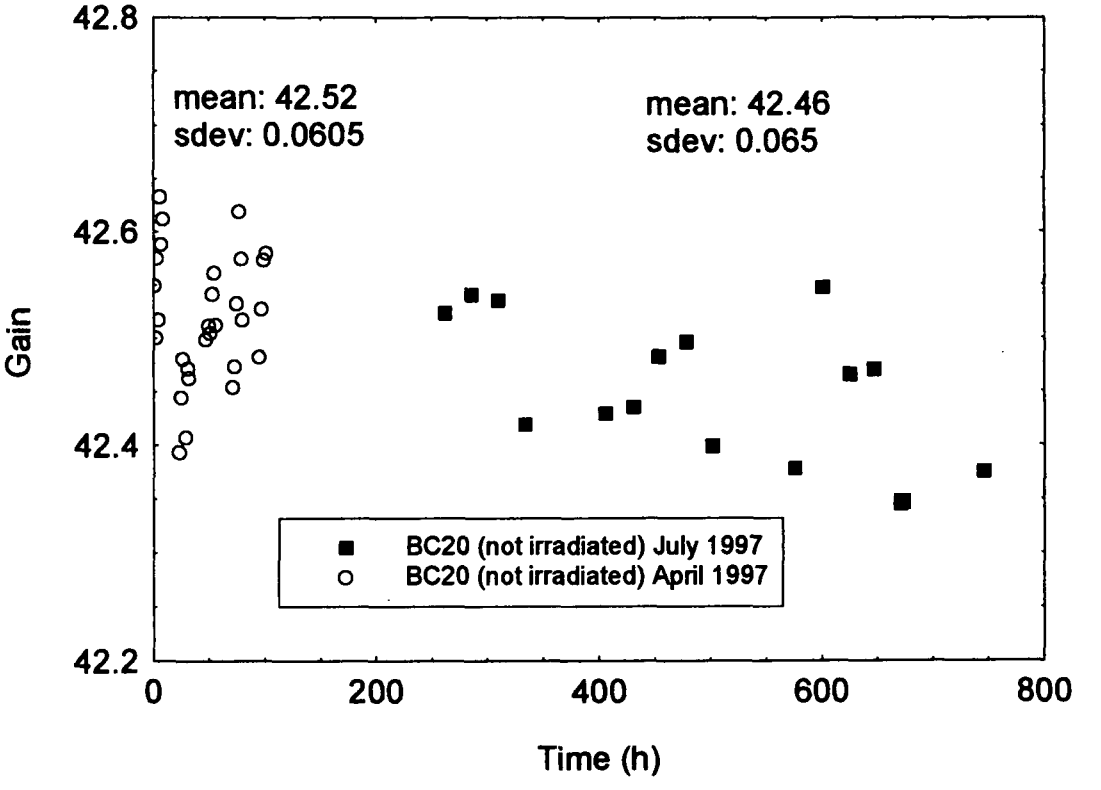

FIGURE 15

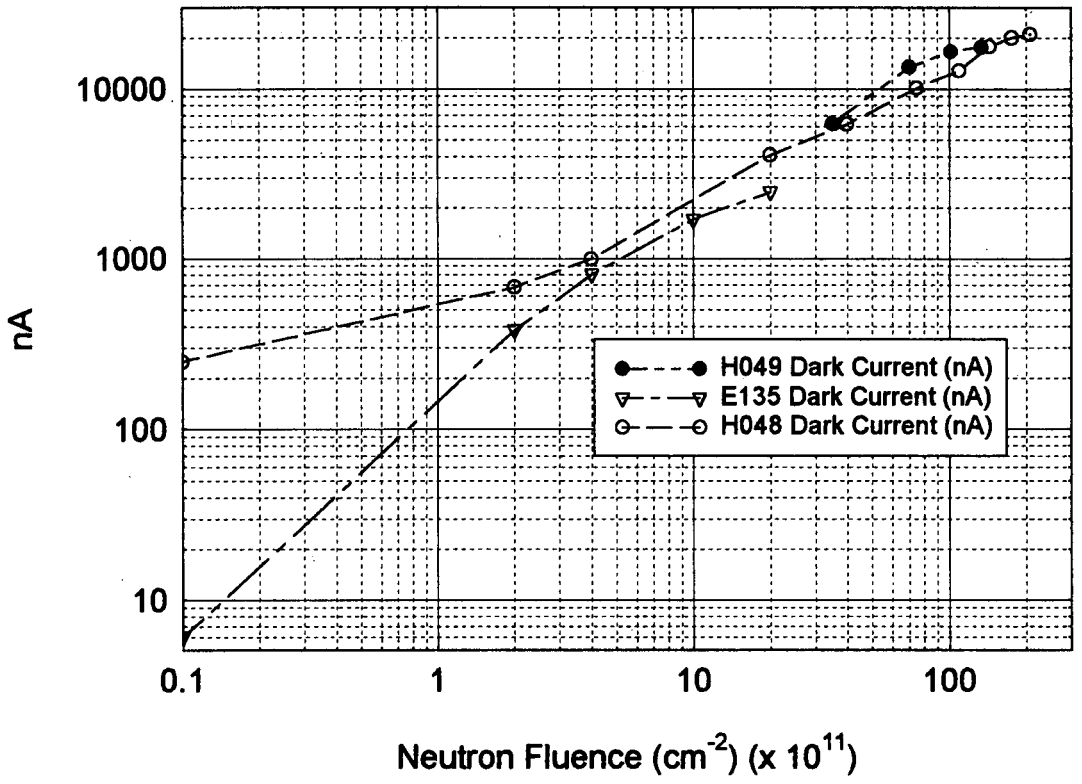

FIGURE 16

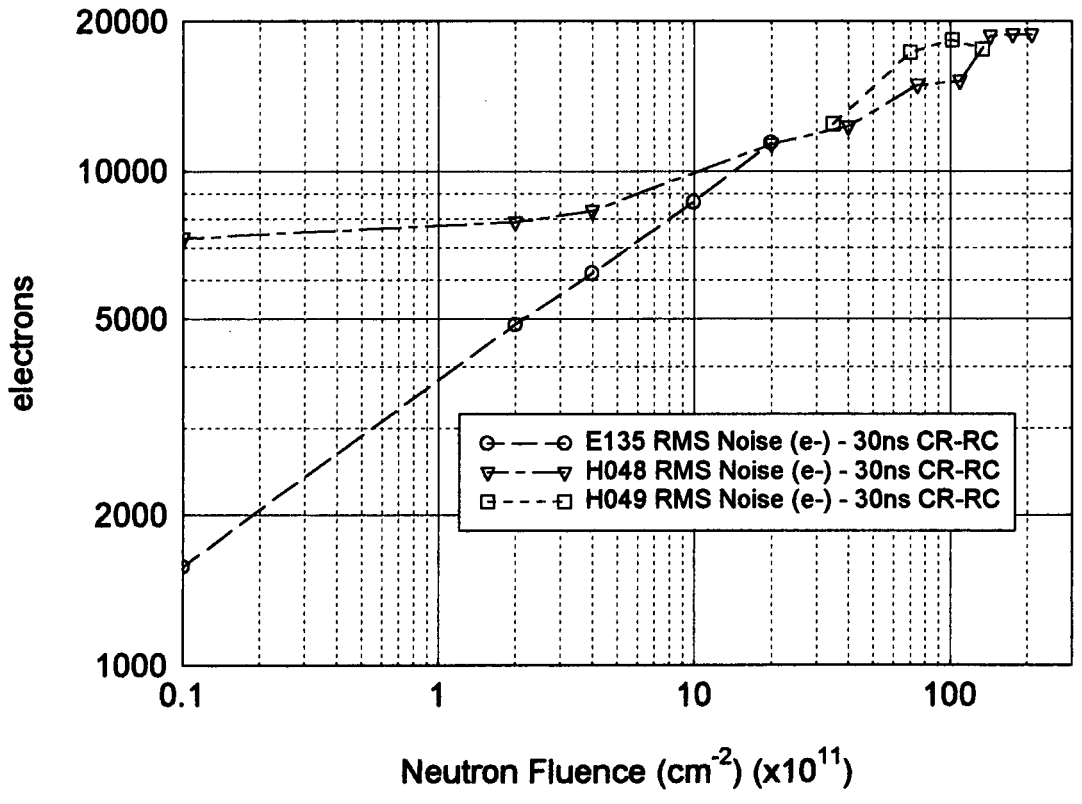

FIGURE 17

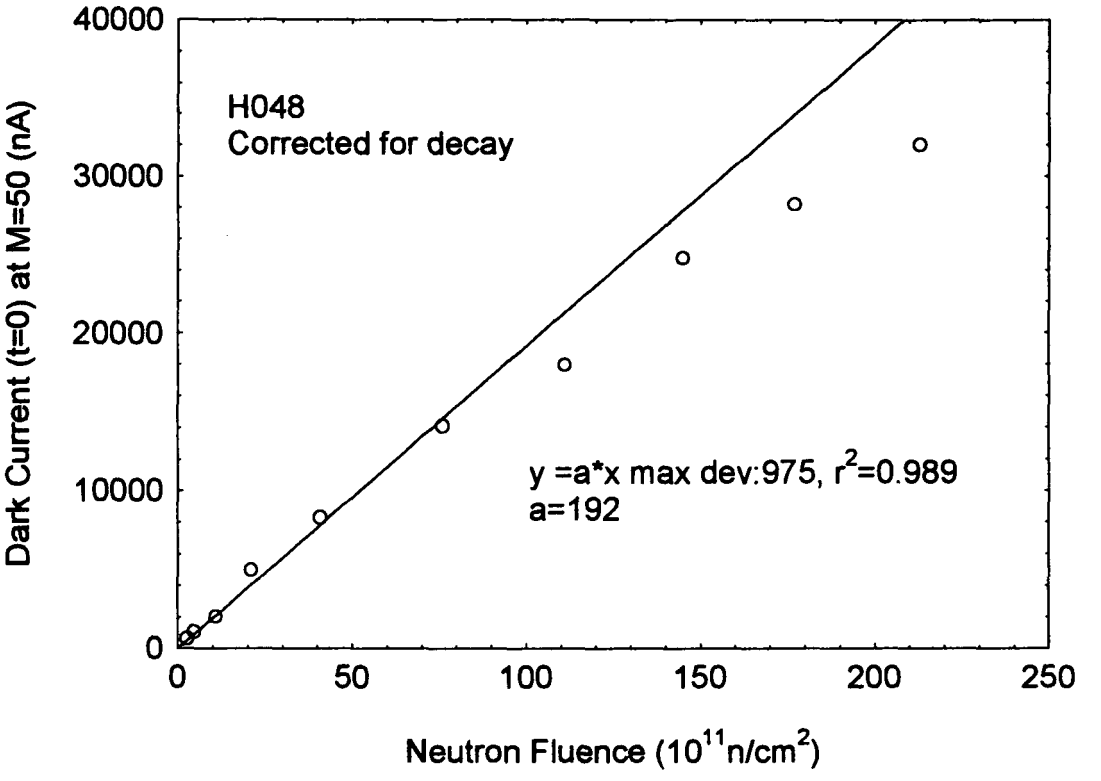

FIGURE 18

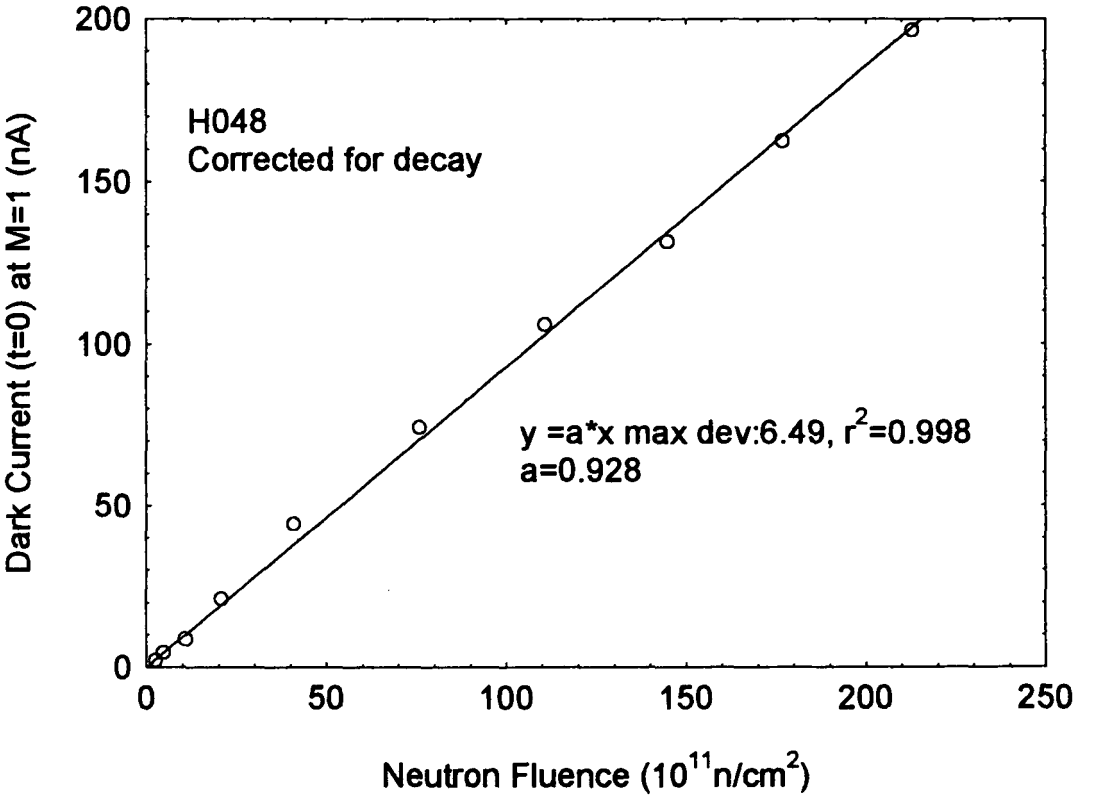

FIGURE 19

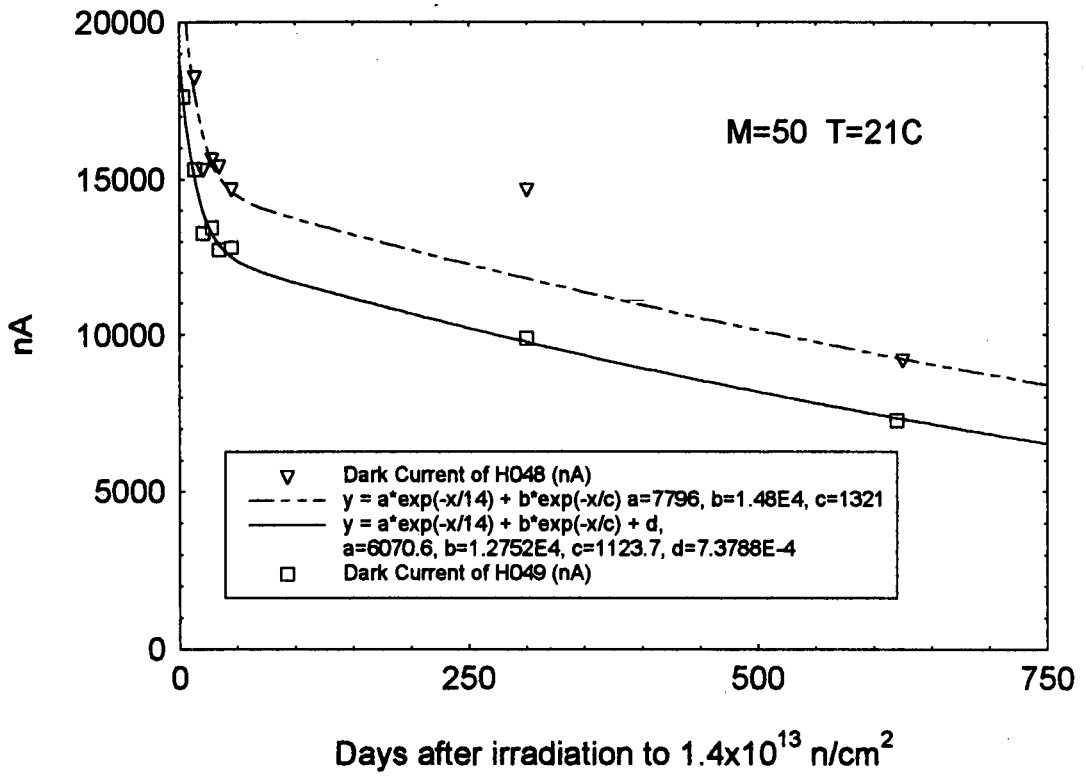

FIGURE 20

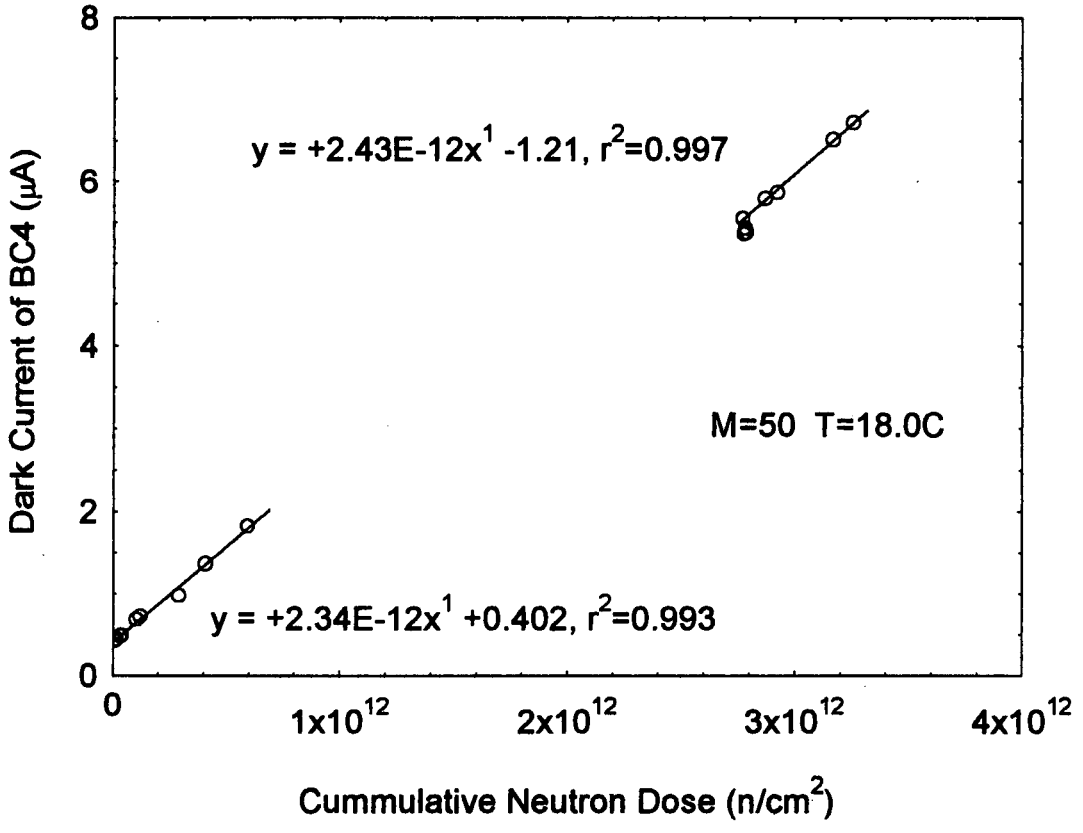

FIGURE 21

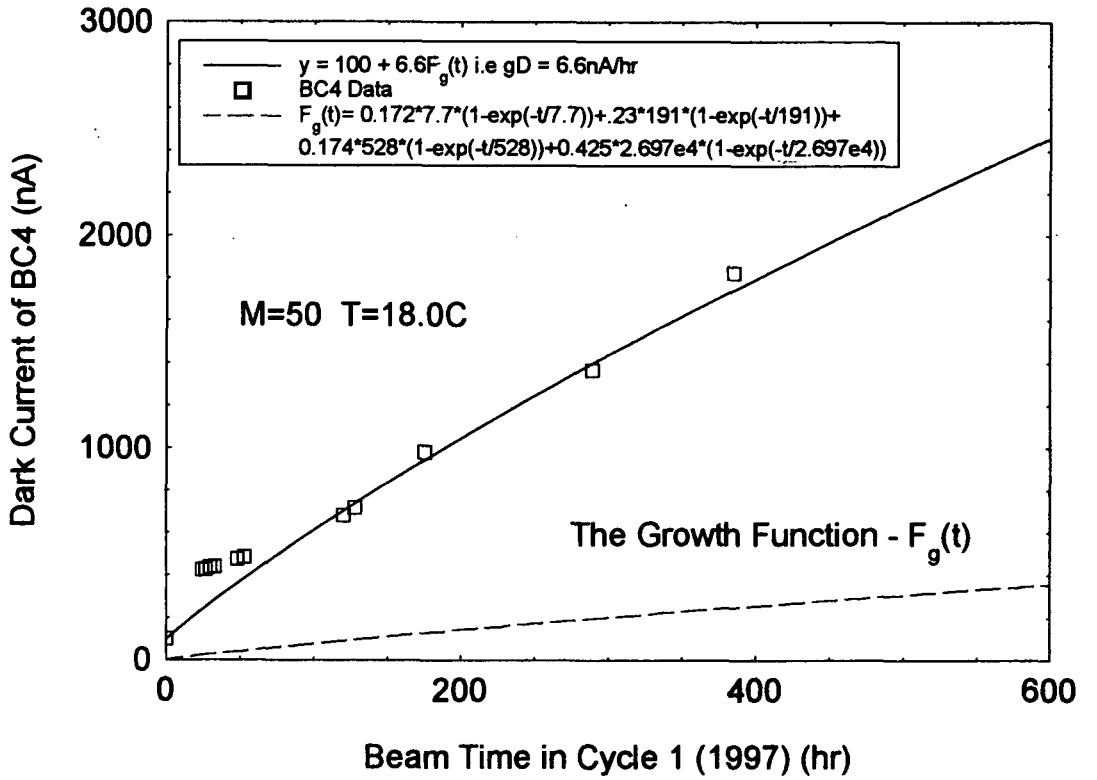

FIGURE 22

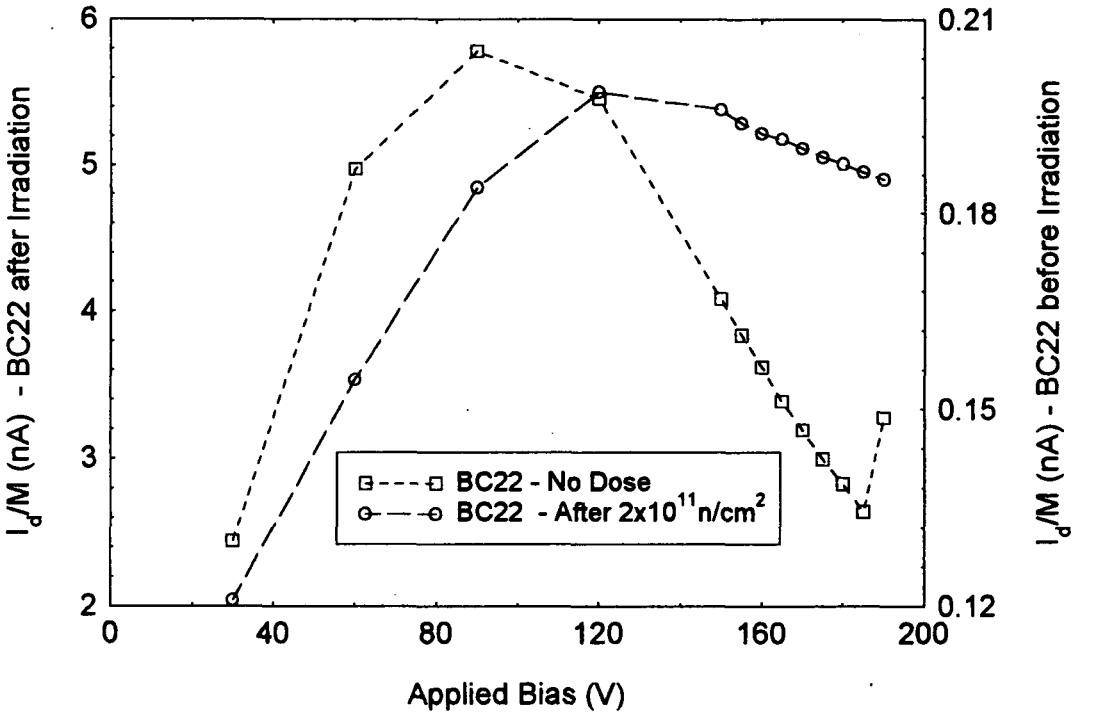

FIGURE 23

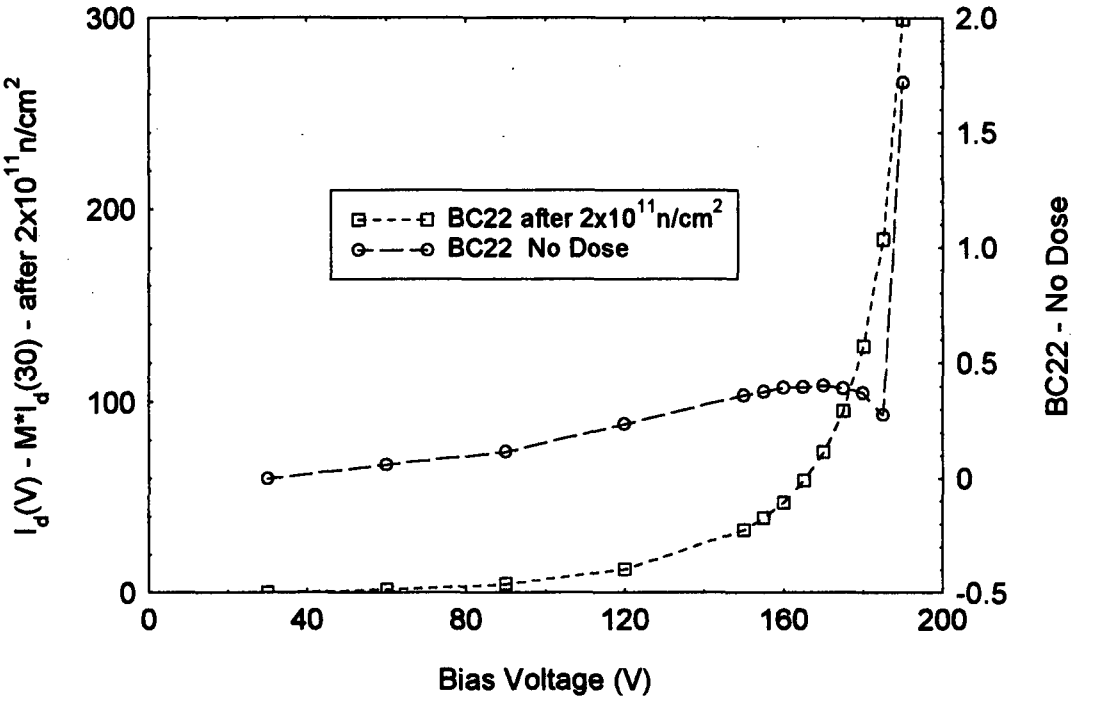

FIGURE 24

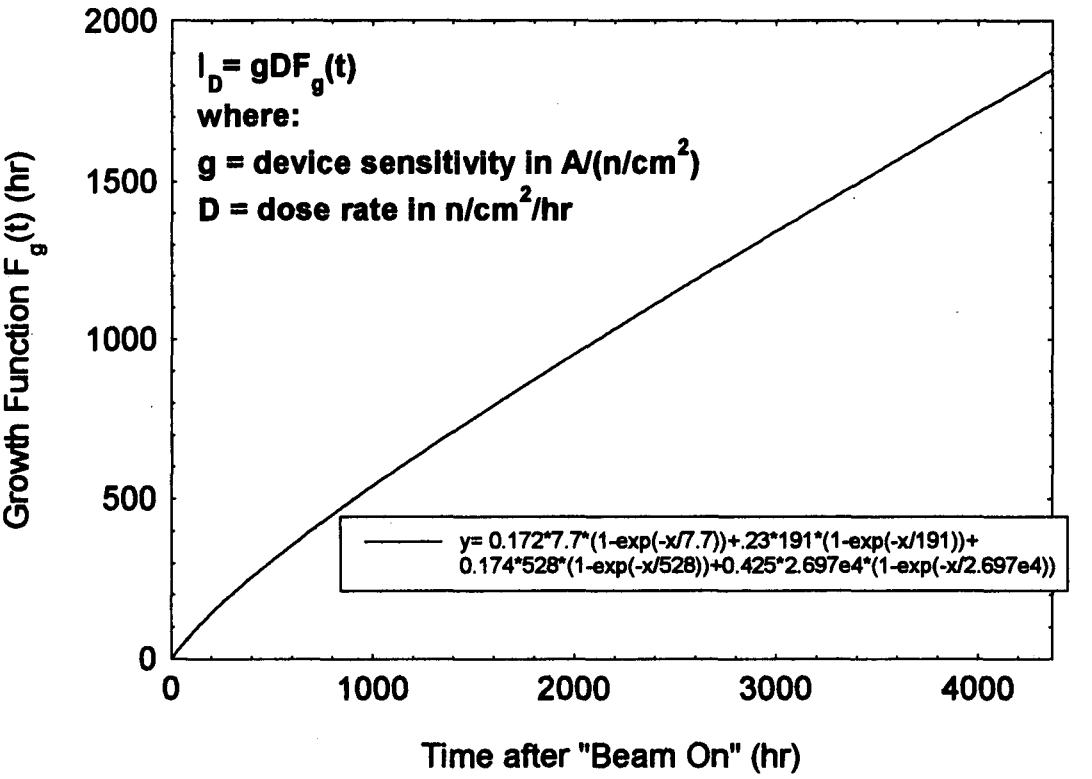

FIGURE 25

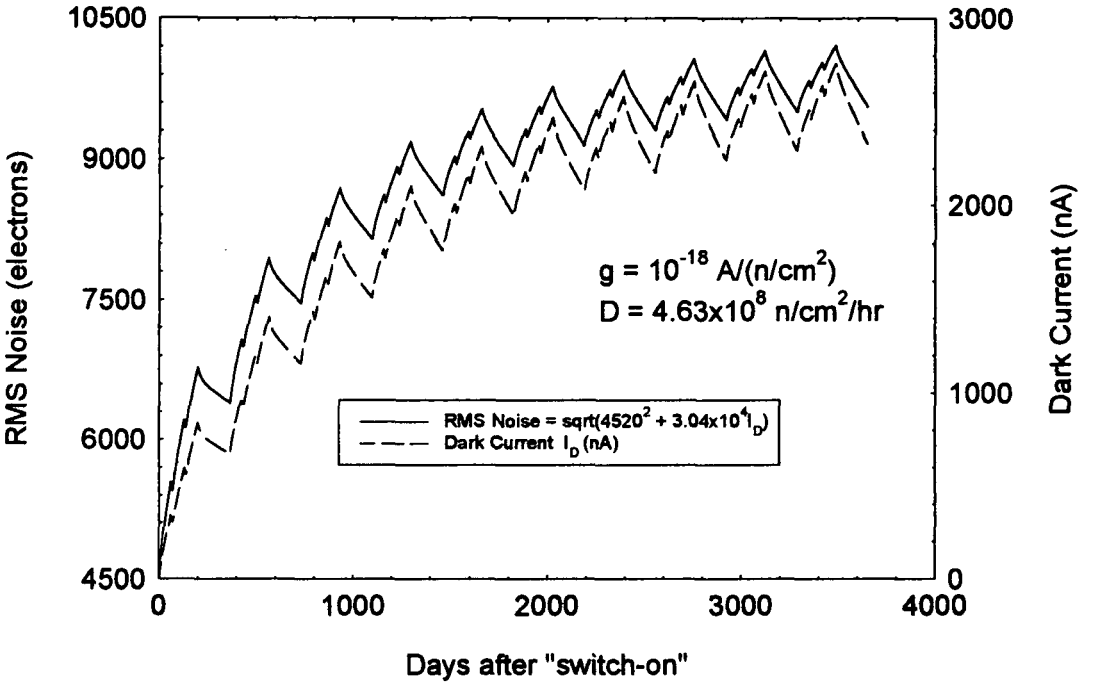

FIGURE 26